TOPICAL REVIEW

Spin-charge interconversion of two-dimensional electron gases at oxide interfaces

View the article online for updates and enhancements.

Topical Review

Spin-charge interconversion of two-dimensional electron gases at oxide interfaces

Dongyao Zheng[1,2] , **Hui Zhang**[1,2,*] , **Fengxia Hu**[3,4] , **Baogen Shen**[3,4,5], **Jirong Sun**[3,4,6] **and Weisheng Zhao**[1,2,*]

[1] School of Integrated Circuit Science and Engineering, Beihang University, Beijing 100191, People's Republic of China
[2] Beijing National Laboratory for Condensed Matter Physics and Institute of Physics, Chinese Academy of Sciences, Beijing 100190, People's Republic of China
[3] School of Physical Sciences, University of Chinese Academy of Sciences, Beijing 100049, People's Republic of China
[4] Ningbo Institute of Materials Technology & Engineering, Chinese Academy of Sciences, Ningbo, Zhejiang, 315201, People's Republic of China
[5] Songshan Lake Materials Laboratory, Dongguan, Guangdong 523808, People's Republic of China
[6] Spintronics Institute, Jinan University, Jinan 343672, Shandong Provence, People's Republic of China

E-mail: huizh@buaa.edu.cn and wszhao@buaa.edu.cn

Abstract
Oxide two-dimensional electron gas (2DEG) is a low-dimensional carrier system formed at the interface of oxide heterojunctions with strong and tunable Rashba spin–orbit coupling which makes oxide 2DEG an ideal platform for converting spin current and charge current. This review provides a summary of the recent advances on the 2DEGs at oxide interfaces for spin-charge interconversion. On one hand, we analyze properties and the efficiency of the spin-to-charge conversion through different ways of spin current injection. On the other hand, the conversion of charge current to spin current under different experimental methods has been summarized. These research achievements provide perspectives and methods for understanding and regulating the spin-charge interconversion of the 2DEG at the oxide interface.

Keywords: spin-charge interconversion, two-dimensional electron gases, oxide interfaces, Rashba spin–orbit coupling

1. Introduction

In 2004, Hwang *et al* reported a high-mobility two-dimensional electron gas (2DEG) at the interface of $LaAlO_3/SrTiO_3$ (LAO/STO), a landmark oxide interface [1]. This spurred intensive research on the origins of 2DEGs, and soon after various STO-based heterointerfaces were fabricated to produce 2DEGs [2–7]. Diverse phenomena have been observed at the interface, including ultrahigh mobility [8], interfacial

magnetism [9] superconductivity [10–12], gate tunable Rashba effect [13–16] and spin-charge interconversion [17–28]. Among them, the latter two effects are particularly attractive in the sense that they provide opportunities to incorporate spin-orbitronic functionalities into 2DEGs.

Various quantum materials including Rashba interfaces (i.e. non-magnetic metal interfaces [29, 30], 2DEGs at insulating oxide interfaces [20, 23], metal-insulating oxide interfaces [31, 32]), topological insulators [33–36], two-dimensional materials (i.e. graphene, two-dimensional metal carbide) [34, 37], and non-collinear antiferromagnets [38, 39] have been used as

---

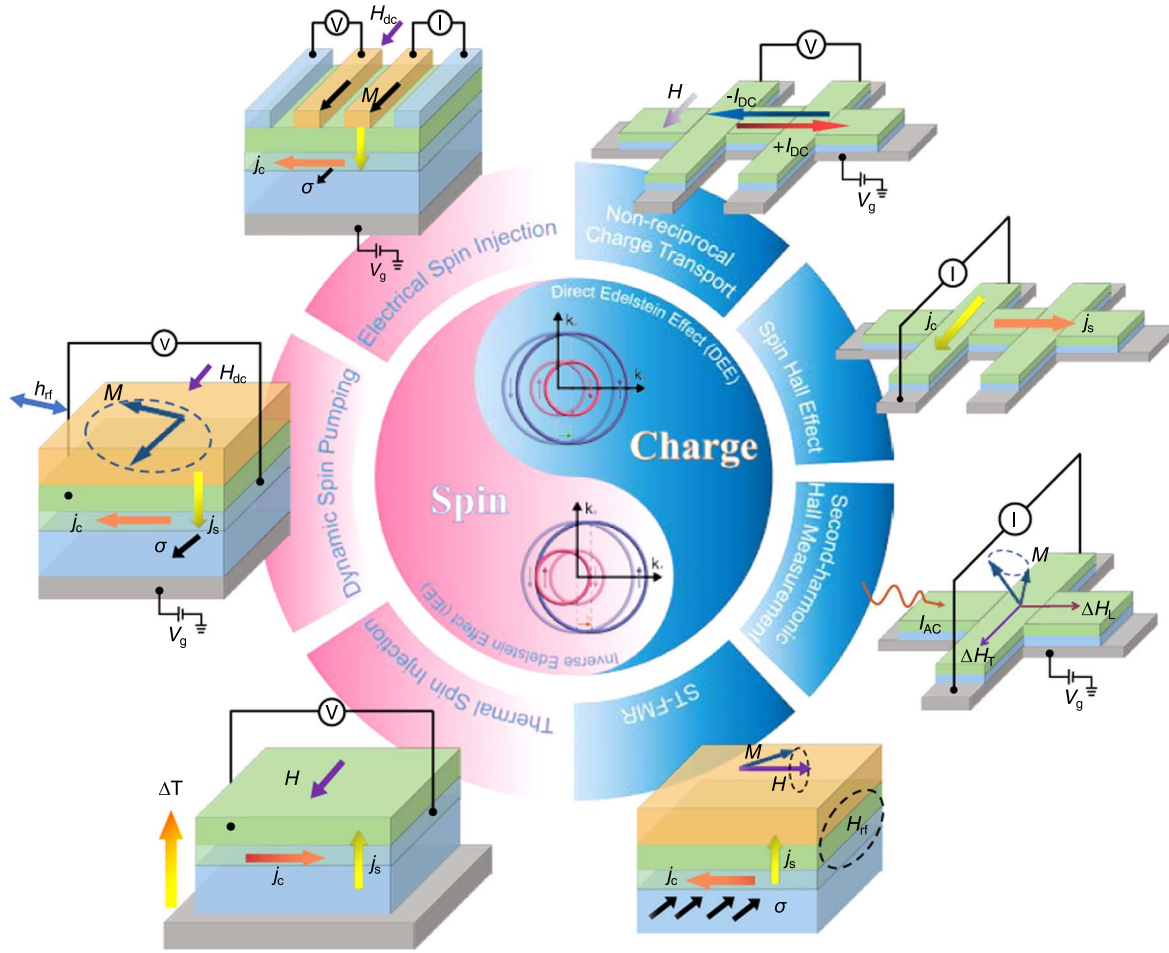* Authors to whom any correspondence should be addressed.

Figure 1. Experimental methods used for the characterization of spin-charge interconversion for 2DEGs at the oxide interfaces.

the source of spin-charge interconversion. Among them, the 2DEGs at oxide interface exhibit efficient spin-charge interconversion, which have aroused wide interest among researchers (figure 1). Owing to Rashba spin–orbit coupling, the 2DEGs at the oxide interface have the characteristic of spin–momentum locking, i.e. both electron momentum and electron spin are constrained to the conductive interface and are locked orthogonally [40, 41]. Through this mechanism, non-equilibrium spin density can be converted into current and vice versa, achieving mutual conversion between spin current and charge current [42, 43]. As a result, the efficiency of charge-spin interconversion is dependent to the strength of the Rashba spin–orbit coupling (SOC). Strong Rashba spin–orbit coupling has been demonstrated at STO-based heterointerfaces [13, 44–46]. In contemporary research, a novel 2DEG is generated at the interface of $KTaO_3$ (KTO) based heterostructures and their surface. Noted that KTO possesses a stronger SOC compared to STO, attributable to the presence of 5d tantalum (Ta) ions in its structure [17, 47, 48]. Higher spin-charge interconversion efficiency is expected to be achieved in KTO systems. In addition, the strength of Rashba spin–orbit coupling can be modulated by external electric fields [49–52]. Therefore, controlling spin–orbit coupling in 2DEG is of great significance for achieving efficient conversion between spin current and charge current.

It is important to note that the direct Edelstein effect (DEE) [42] refers to the phenomenon in spin–orbit coupling materials where a perpendicular electric field induces spin polarization that is perpendicular to the field direction and charge polarization that is parallel to the field direction. Figure 2(a) shows the sketch of a simplified Rashba-type system at equilibrium, which illustrates dispersion relations of LAO/STO system [20]. At the Fermi level, there are two Fermi contours with opposite spin textures (the spin direction of electrons on the outer contour is opposite to that on the inner contour). As shown in the top panel of figure 2(b), when an in-plane electric field is applied along the positive direction of vector k_x, due to spin–momentum locking, the Fermi circle will move a distance of Δk in the opposite direction, causing a non-equilibrium spin accumulation and promoting the conversion of charge current to spin current [53]. DEE leads to the generation of spin current induced by a charge current flowing in inversion antisymmetric 2DEGs [53] as described by the following relation:

$$J_S \propto \alpha_R (\hbar/e)(z \times J_C), \tag{1}$$

where J_S is the spin-current, α_R is the Rashba parameter, z is the interfacial electric field direction perpendicular to the 2DEGs, and J_C is the charge current. The efficiency of
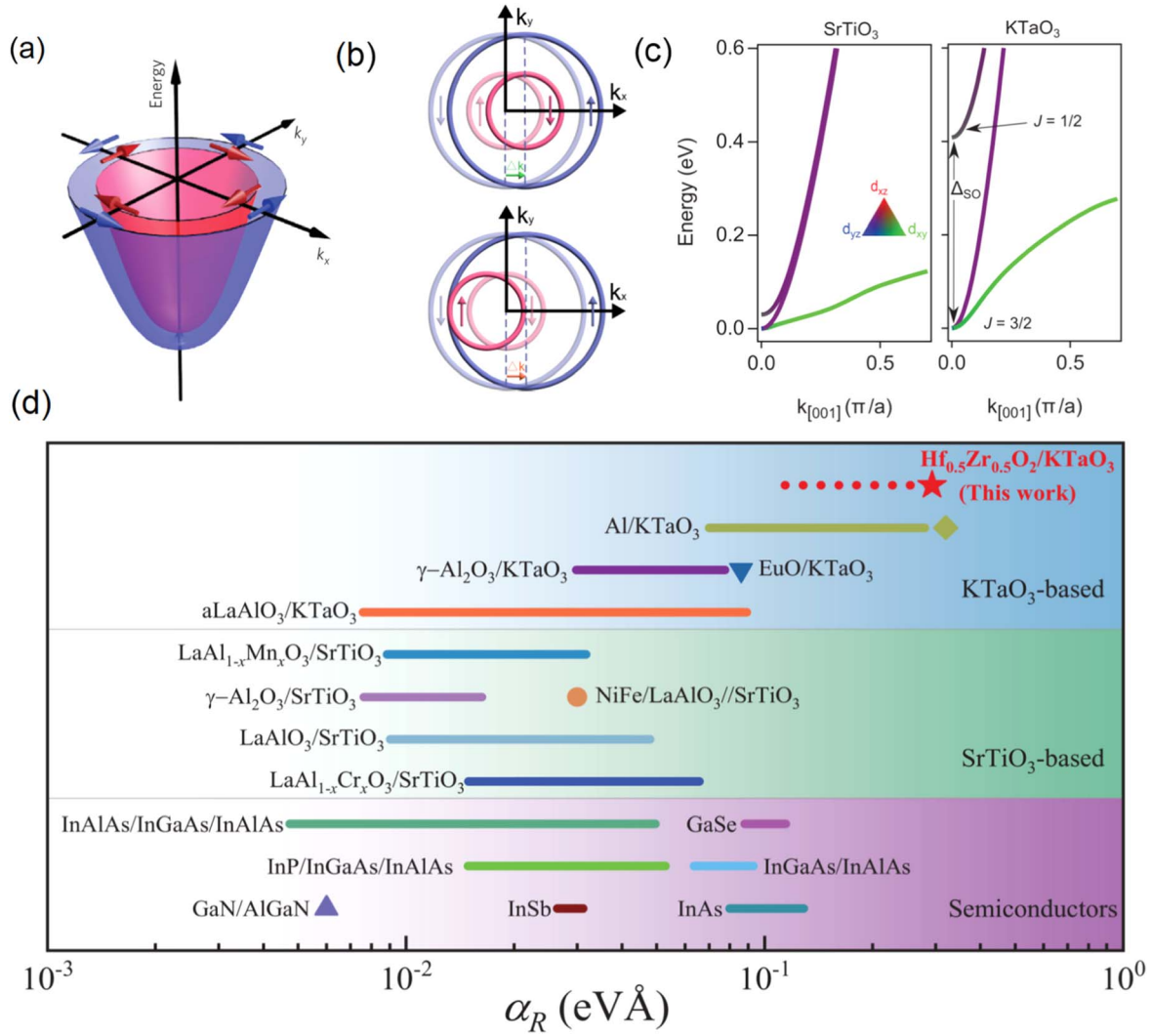
Figure 2. (a) Sketch of a Rashba-type system at equilibrium. Reproduced from [20], with permission from Springer Nature. (b) Diagram for the Fermi profile of the Direct Edelstein effect (DEE) and Inverse Edelstein effect (IEE). (c) The bulk band structure of SrTiO$_3$ and KTaO$_3$. [47] John Wiley & Sons. © 2019 WILEY-VCH Verlag GmbH & Co. KGaA, Weinheim. (d) Rashba coefficients for Al/KTaO$_3$ with g-factor of 0.5–2 [17] and the related value extracted from ARPES is marked as rhombus [54], γ-Al$_2$O$_3$/KTaO$_3$ [48], Hf$_{0.5}$Zr$_{0.5}$O$_2$/KTaO$_3$ [55], EuO/KTaO$_3$ [56], aLaAlO$_3$/KTaO$_3$ [52],) STO-based 2DEG (LaAl$_{1-x}$Mn$_x$O$_3$/SrTiO$_3$ ($0 \leqslant x \leqslant 1$) [49], γ-Al$_2O_3$/SrTiO$_3$ [57], LaAlO$_3$/SrTiO$_3$ [13], LaAl$_{1-x}$Cr$_x$O$_3$/SrTiO$_3$ ($x = 0, 0.1, 0.2$) [58], NiFe/LAO/STO [20]) and semiconductors (InAlAs/InGaAs/InAlAs [59], GaSe [60], InP/InGaAs/InAlAs [58], InGaAs/InAlAs [61], GaN/AlGaN [62], InSb [63], InAs [64]. [55] John Wiley & Sons. © 2023 Wiley-VCH GmbH.

charge-to-spin conversion is represented by:

$$\theta_{CS} = \frac{J_S}{J_C}. \qquad (2)$$

On the contrary, the inverse Edelstein effect (IEE) [43, 65] describes the phenomenon of charge accumulation resulting from the injection of spin-polarized current into spin–orbit coupled materials. As shown in the bottom panel of figure 2(b), when a perpendicular spin current is injected into the 2DEG, it induces a change in momentum space accordingly. Therefore, a lateral charge current is converted at the interface [42]. IEE length (λ_{IEE}), which serves as a critical parameter in characterizing the inverse Edelstein effect, represents the distribution length of the charge accumulation, i.e. the diffusion distance of charges. The spin-to-charge

conversion efficiency is typically characterized by λ_{IEE}:

$$\lambda_{IEE} = \frac{J_C}{J_S} = \frac{\alpha_R \tau}{\hbar} \qquad (3)$$

with α_R representing the Rashba coefficient, τ representing momentum/spin relaxation time, J_S representing the spin current and J_C representing the charge current [33, 66]. Generally, a larger λ_{IEE} implies that charge accumulation can diffuse over a greater distance within the material, resulting in a higher efficiency of spin-to-charge conversion [29].

This review introduces the latest progress in research on spin-charge interconversion based on the 2DEG at the oxide interface, as shown in figure 1. We talk about the strong Rashba spin–orbit coupling in the oxide 2DEG and its controllable properties, which is the origin of spin-charge interconversion in oxide 2DEG. Based on this, we discuss the

conversion from spin current to charge current through different injection methods of spin current, including electrical spin injection, dynamic spin pumping and thermal spin injection. Additionally, we focus on the characterization methods of conversion from charge current to spin current, such as spin torque ferromagnetic resonance (ST-FMR), second-harmonic Hall measurement, non-reciprocal charge transport and double Hall bar nonlocal measurements. Researchers devote to explore material systems to seek higher spin-charge conversion efficiencies. Simultaneously, they should search for more effective methods to control external fields in order to achieve precise modulation of the spin-charge conversion process.

2. Rashba spin–orbit coupling of 2DEGs

At the heterointerface of oxides, the Rashba SOC phenomenon can facilitate an efficient transformation between spin current and charge current. Furthermore, the strength of Rashba spin–orbit coupling can be modulated by external multistimuli, including electrical fields [49–52], allowing for the manipulation of electronic states on-demand at the oxide interfaces. Therefore, tuning spin–orbit coupling of 2DEGs is of great significance for achieving highly efficient conversion between spin and charge currents [67].

2.1. Strong Rashba spin–orbit coupling

Due to the confinement of electrons in a two-dimensional interface and the breaking of inversion symmetry, interfacial electrons are exclusively accumulated on the 3d electronic shell of the Ti ions, residing in the t_{2g} conduction bands of STO. Quantum confinement lifts the orbital degeneracy of the bulk band structure and leads to the hierarchic band structure of 2DEGs. Under the effect of spin–orbit interaction, the splitting of the d_{xy} and d_{xz} and/or d_{yz} orbitals occurs, lifting the degeneracy of the electronic states and resulting in sizable Rashba spin splitting, which is enhanced by orbital hybridization [44, 45, 68]. As evidenced by theoretical calculation, the strong dependence of the charge-to-spin conversion on the Fermi level originates from the Rashba spin splitting of the hierarchic band structure, and the enhanced spin splitting due to orbital hybridization leads to the highest conversion efficiency when the Lifshitz transition occurs [44, 45, 55]. Notably, the observed Lifshitz transition occurs when the emergence of a second species of charge carriers occupying the d_{xz} and/or d_{yz} orbital states [69–71]. The direct visualization of Rashba-split bands, using angle-resolved photoemission spectroscopy (ARPES), has predicted a highly efficient spin-charge interconversion [46, 72, 73].

Compared with 3d transition metal oxide STO, the uniqueness of KTO as a 5d transition metal oxide lies in its stronger atomic spin–orbit interaction [74, 75]. The bulk band structures of STO and KTO are shown in figure 2(c), the spin splitting energy Δ_{so} is ~ 0.02 eV for the Ti 3d electrons in STO, while ~ 0.4 eV for the Ta 5d electrons, which is almost 20 times than that of STO [47]. Many researchers have investigated KTO-based oxide 2DEGs to obtain a larger Rashba coefficient ($\alpha_R = \Delta_{so}/2k_F$ where k_F is Fermi wave vectors). The largest Rashba coefficient currently discovered by researchers comes from Al/KTaO$_3$ [17], where $\alpha_R = 0.32$ eVÅ, extracted from the angle-resolved photoemission spectroscopy in (001) orientation [48]. Figure 2(d) illustrates a comparison of the extracted Rashba coefficients in different systems including traditional semiconductor 2DEGs, STO-based oxide 2DEGs and KTO-based oxide 2DEGs [55], indicating that compared with traditional semiconductors 2DEGs and STO-based oxide 2DEGs systems, the KTO-based oxide 2DEGs system has a larger Rashba coefficient [17, 20, 48, 49, 52, 54, 56–64, 76]. Therefore, it is expected that a higher spin-charge interconversion efficiency will be achieved in KTO-based 2DEGs systems [77, 78].

2.2. Electric field tunable of SOC

Different from conventional semiconductor 2DEGs, oxide 2DEGs have a large Rashba spin–orbit interaction, whose magnitude can be modulated by the application of an external electric field [13]. Extensive efforts have been made to tune the Rashba field and other novel properties for 2DEGs at oxide interfaces by electrostatic gating [49–51, 79, 80]. Conventional electric field effect to tune properties requires high voltages of tens to hundreds of volts, which is also called back-gate voltage modulation. Caviglia *et al* [13] successfully achieved effective control of the Rashba SOC by applying gate voltage at the LAO/STO interface. As shown in figures 3(a) and (b), through quantitative analysis of weak anti-localization of the LAO/STO interface 2DEG under different gate voltages, Caviglia *et al* [13] investigated the influence of gate voltage on the strength of Rashba SOC and proposed that the field effect on the critical temperature of superconductivity is due to the field effect on the strength of spin–orbit coupling (figure 3(c)). Besides LAO/STO system [13, 71, 81–83], back-gate voltage modulation has also been explored massively in other systems, such as LaVO$_3$/SrTiO$_3$ [84], EuO/KTO [56] and LAO/KTO [50]. Different from the studies with conventional electric field effects, the electric double layer transistor (EDLT) with an ionic liquid (IL) as the dielectric layer provides a more powerful means to tune the carrier density and Hall mobility with only a few volts [85–87]. Figure 3(d) illustrates the basic mechanism of EDLT at the γ-Al$_2$O$_3$/SrTiO$_3$ (GAO/STO) interface and figure 3(e) shows the gate voltage dependence of the contribution of spin–orbit interaction and inelastic scattering, which shed light on the modulation of spin–orbit interaction [14].

3. Spin-to-charge conversion in 2DEGs

The conversion of spin current to charge current enables the detection and manipulation of electron spin states [88]. Similar to the spin-to-charge conversion at topological insulator interfaces [35], the spin-to-charge conversion for 2DEG at the oxide interface has a series of characteristics, such as high effective conversion efficiency and gate tunability,
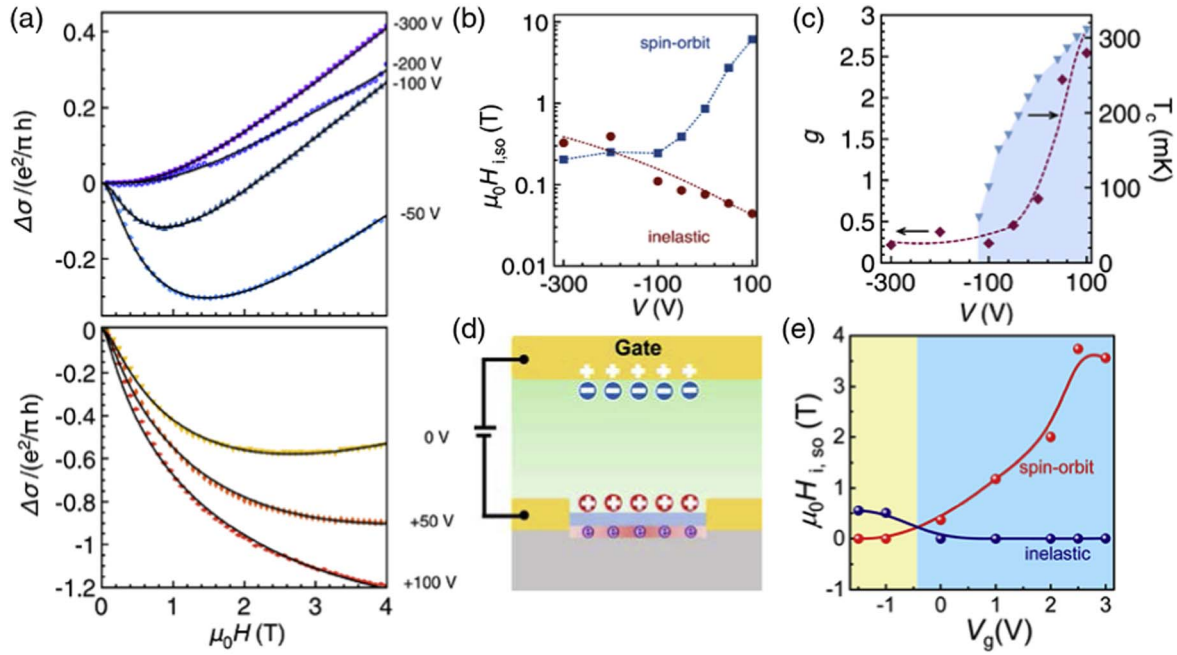
Figure 3. (a) Weak anti-localization of the LAO/STO interface at different back-gate voltages. (b) Back-gate voltage tunable Rashba SOC of the LAO/STO interface. (c) Back-gate voltage dependence of the electrons factor g and superconducting critical temperature T_c. Reprinted (figure) with permission from [13], Copyright (2010) by the American Physical Society. (d) Basic mechanism of EDLT under applied positive voltages. (e) Gate voltage tunable Rashba SOC of the γ-Al$_2$O$_3$/SrTiO$_3$ interface. Reprinted with permission from [14]. Copyright (2017) American Chemical Society.

which may facilitate the development of novel technologies such as spin-based memory and logic devices. λ_{IEE} is the figure of merit characterizing the efficiency of spin-to-charge conversion. λ_{IEE} of Rashba interfaces are measured at room temperature (0.1–0.4 nm for Bi/Ag [29, 89]), topological insulator surfaces (2.1 nm for α-Sn [43]), heavy metals (0.2 nm for Pt, 0.3 nm for Ta and 0.43 nm for W) while that of 2DEGs are measured at low temperature (e.g. 6.4 nm for LAO/STO). Therefore, researchers have done a lot of research to explore the higher conversion efficiency in 2DEG. Three main methods have been explored to inject spin current, namely electrical spin injection, dynamic spin pumping and thermal spin injection.

3.1. Electrical spin injection

In 2012, Reyren *et al* [90] demonstrate efficient electrical spin injection at the LAO/STO oxide interface via Hanle measurements [91, 92], which also gives information on the spin lifetime. The Hanle effect (inverse Hanle effect) is a phenomenon where the precession of spin accumulation is influenced by a perpendicular or transverse magnetic field. When an external magnetic field is applied perpendicularly (parallel) to the magnetization of the ferromagnetic spin injector, spin accumulation is suppressed (restored). Reyren *et al* [90] utilized a nonlocal, 3-terminal configuration for spin injection into the 2DEGs at the interface, as shown in figure 4(a). They analyzed the voltage changes associated with the spin accumulation dynamics driven by vertical or transverse magnetic fields (Hanle and inverse Hanle effects) and the modulation of the density of states at the quasi-two-

dimensional electron system (2-DES) interface using back-gate voltage. Figure 4(b) demonstrates the Hanle and inverse Hanle effects under back-gate voltage modulation. The influence of bias and back-gate voltages reveals that the spin accumulation signal is amplified by resonant tunneling through localized states in the LAO strongly coupled to the 2-DES by tunneling transfer. It is worth noting that the total amplitude of the Hanle signal $\Delta R_H A$ is observed to be larger by five to six orders of magnitude than the theoretically estimated value [93]. They attributed this large amplitude to resonant spin injection tunneling transmission [90]. However, Inoue *et al* later provided an alternative explanation for the similar magnetoresistance (MR) phenomenon observed at the Co/LAO/Nb:STO interface (figure 4(d)), which differed from the Hanle effect [94]. They gave a different interpretation to the observed MR (figure 4(c)) and assigned the origin of the magnetoresistance to spin-dependent hopping through defect states in the barrier [94]. They have questioned the reliability of explaining the Hanle effect in a three-terminal geometric structure and have raised doubts about the derived spin lifetime which is characterized by the observed MR in ferromagnet-nonmagnet tunnel junctions.

3.2. Dynamic spin pumping

In contrast to conventional electrical spin injection, the technique of spin pumping injection, as reported by Lesne *et al* [20], offers advantages in terms of enhanced detectability of electrical signals, compatibility with gate control, and convenience for investigating the efficiency of spin-to-charge conversion at oxide interfaces. Numerous research groups
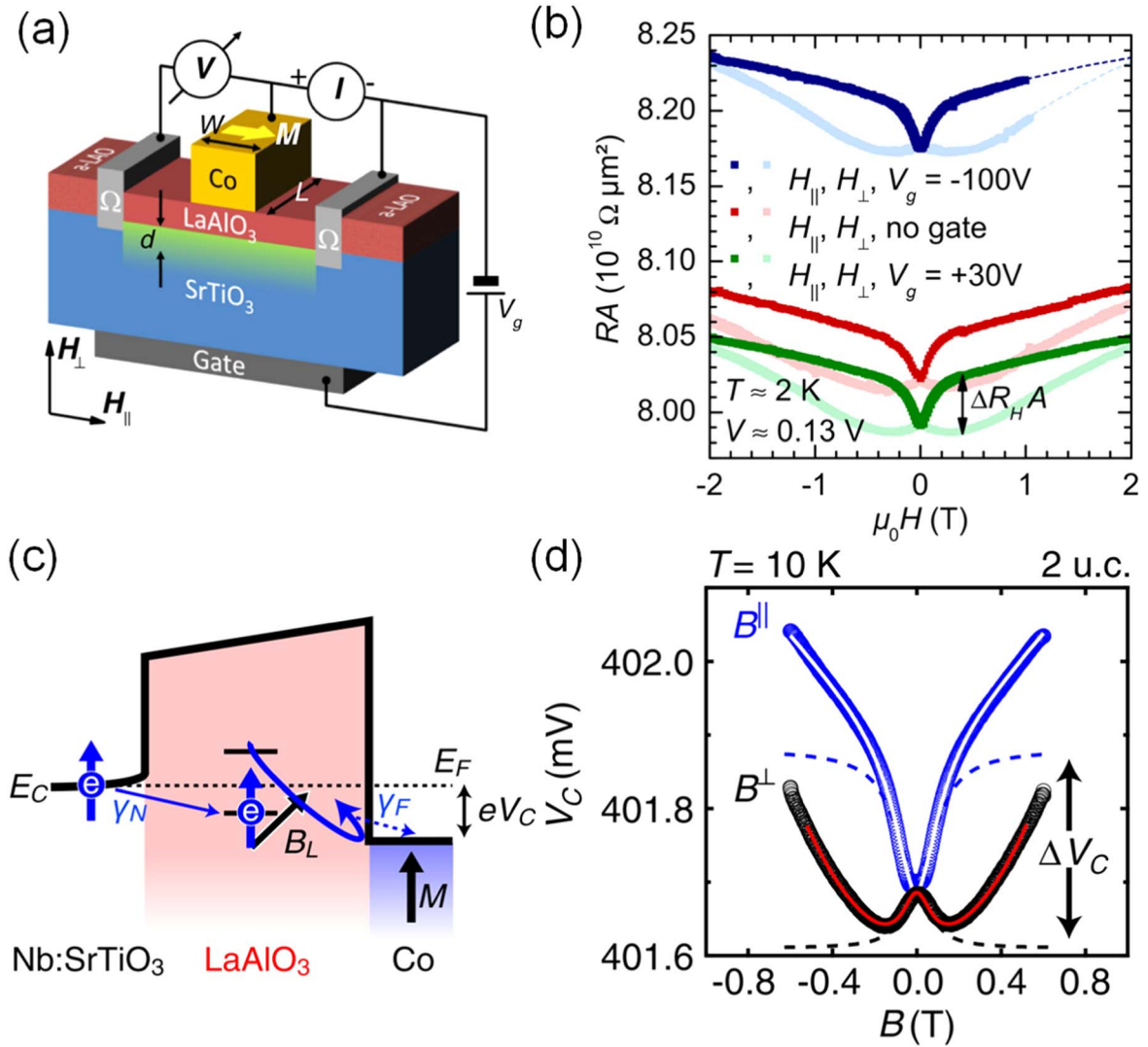
Figure 4. (a) Sketch of the configuration for the electrical spin injection into the LAO/STO 2DEG. (b) Hanle and inverted Hanle data acquired at 2 K with different gate voltage V_g. Reprinted (figure) with permission from [90], Copyright (2012) by the American Physical Society. (c) Schematic diagram for electron hopping through LAO. (d) Representative junction MR under perpendicular and parallel magnetic fields. Reproduced from [94]. CC BY 3.0.

have successfully employed this dynamic spin pumping technique to introduce spin-polarized currents into 2DEGs at oxide interfaces [17, 20, 25, 47]. As shown in figure 5(a), Lesne *et al* [20] first reported significant spin-to-charge conversion for the 2DEG at the LAO/STO interface, spin pumping drives the magnetization of a ferromagnetic layer (e.g. NiFe) into precession by applying an external magnetic field and radio frequency microwaves together. When resonance conditions are reached, angular momentum is ejected from the NiFe layer, then spin-polarized carriers accumulate at the interface between the ferromagnet and channel layer. Through ferromagnetic resonance (FMR) measurement, spin-polarized current is pumped into 2DEGs, and then charge accumulates through IEE; thus, a voltage signal (V_{IEE}) can be recorded, as shown in figure 5(b). Figure 5(c) shows the gate dependence of λ_{IEE}, from which a crossover between positive to negative spin-to-charge conversion is clearly visible near $V_g = 0$. It was found that the amplitude of the conversion

current can be modulated by more than an order of magnitude when a gate voltage is applied, and even its sign can be changed, so the efficiency of spin-to-charge conversion also shows gate tunability, which researchers attribute to the huge tunability of Rashba SOC. In their system, λ_{IEE} is as high as -6.4 nm at 7 K and decreases with increasing temperature. In a study conducted by Vaz *et al* [25], a significant enhancement in spin-to-charge conversion efficiency was observed in the AlO_x/STO 2DEG at low temperatures. The correlation between the magnitude of the conversion and the gate-tunable electronic structure was elucidated and presented in figure 5(d). Furthermore, figure 5(e) depicts the dependence of the λ_{IEE} on the applied gate voltage. The spin-to-charge conversion varies strongly in sign and amplitude, with its sign changing several times in the studied range of gate voltages. Moreover, the conversion efficiencies at maximum values are extremely high for both positive and negative values ($+28$ nm, -16 nm). Note that λ_{IEE} is proportional to the
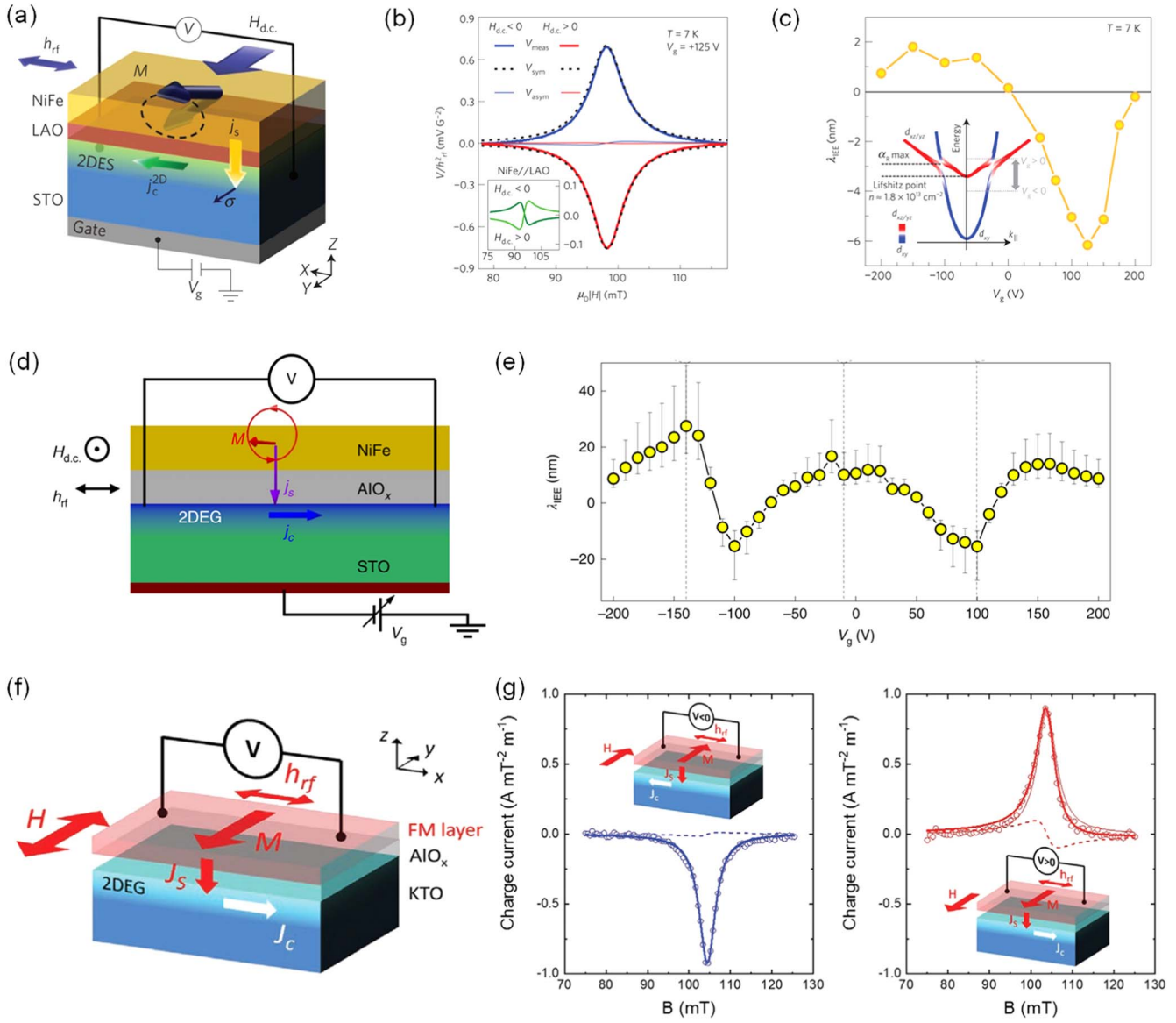
Figure 5. (a) Configuration for the spin-pumping of FMR measurement at LAO/STO interfaces. (b) Converted charge induced voltage at different external magnetic fields. (c) Gate tunable efficiency of the spin-to-charge conversion in the 2DEG at LAO/STO heterointerface. Reproduced from [20], with permission from Springer Nature. (d) Sketch of the spin-pumping experiment at AlO_x/STO interfaces. (e) Gate-tunable efficiency of the spin-to-charge conversion in the heterointerface of AlO_x/STO. Reproduced from [25], with permission from Springer Nature. (f) Detection of the inverse Edelstein effect at AlO_x/KTO interfaces. (g) Results of the SP-FMR measurements of AlO_x/ KTO. Corresponding charge current produced transverse to the magnetization for positive and negative magnetic fields. [17] John Wiley & Sons. © 2021 Wiley-VCH GmbH.

Rashba orbit splitting. This amplified λ_{IEE} is due to the enhanced Rashba-like splitting in the vacant band crossing regime with a nontrivial topology. In addition to the STO-based 2DEG system, another promising oxide system with spin-to-charge conversion potential is KTO-based 2DEG. As analyzed above, Ta is a 5d element that is heavier than Ti, so KTO is expected to have a larger spin–orbit coupling [47]. Recently, Vicente-Arche *et al* synthesized a new Rashba 2D electron gas by depositing aluminum on a KTO substrate (figure 5(f)) [17]. This material stands out as the sole demonstrator of effective spin-to-charge conversion through spin pumping. The spin pumping ferromagnetic resonance (SP-FMR) results, as depicted in figure 5(g), reveal a value of

λ_{IEE} around -3.5 nm at 10 K. This finding is comparable to the measurements conducted on LAO/STO 2DEGs [20, 22, 95], which exhibited values ranging from 2 to -6.4 nm based on gate voltage. Moreover, it represents one of the largest values reported thus far, albeit lower than that observed in AlO_x/STO [25] ($\lambda_{IEE} \approx 30$ nm). It is noteworthy that the resulting raw current is in the magnitude of 40 nA, significantly surpassing the value of 1 nA reported in thermal spin injection experiments [18].

More recently, the Bibes's group [21] proposed a method to suppress power consumption by coupling the ferroelectric properties with spin-to-charge conversion in oxide 2DEG. The polarization of a ferroelectric can be switched by an
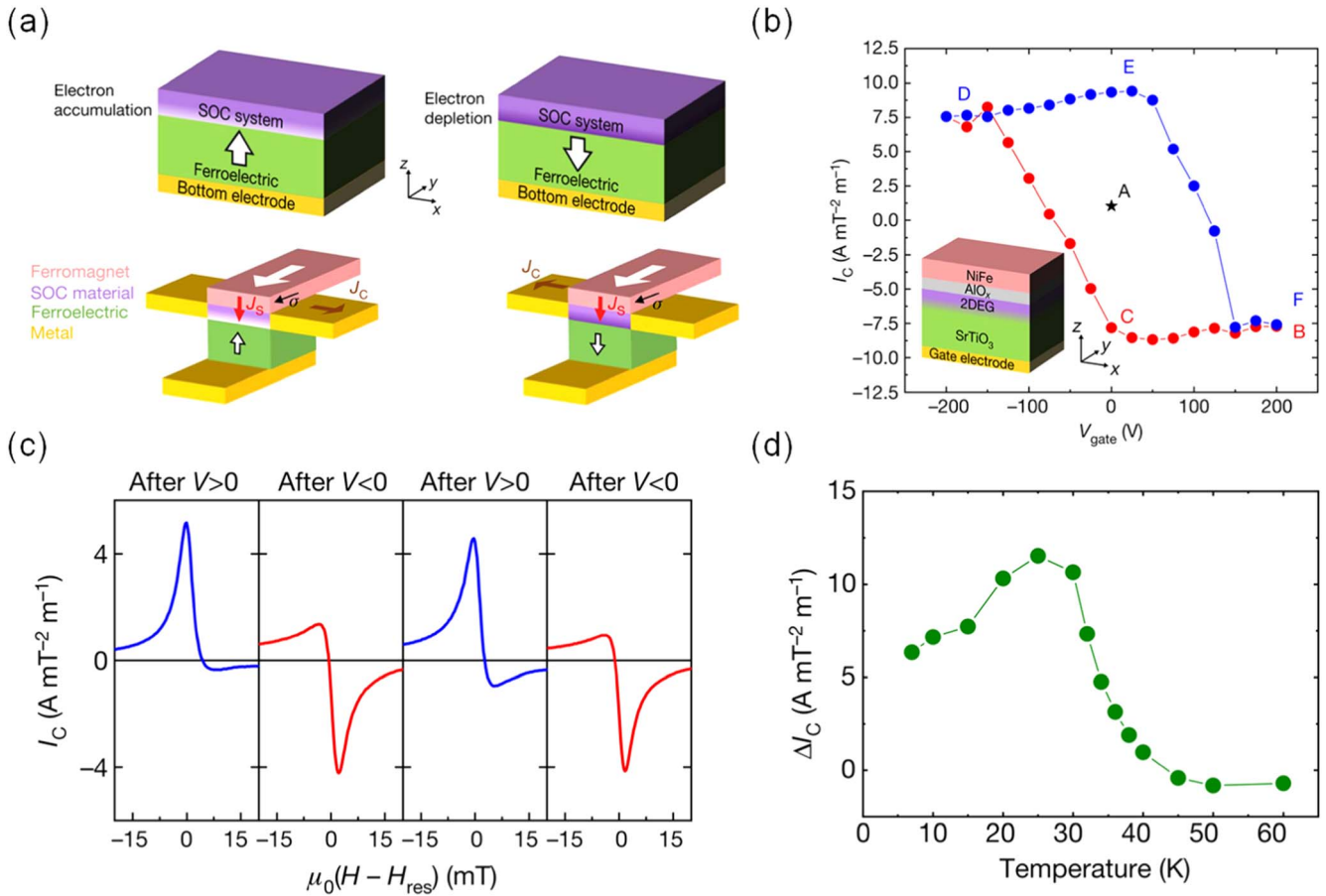
Figure 6. (a) The fundamental principle underlying the manipulation of spin and charge current through ferroelectricity-mediated mechanisms. (b) Converted charge current as a function of the gate voltages. (c) Normalized charge current produced at electrical remanence after applying positive or negative voltage pulses. (d) Temperature-dependent normalized currents. Reproduced from [21]. CC BY 4.0.

electric field, typically at an energy cost 1000 times smaller than that of switching a ferromagnet [96]. In addition, ferroelectrics can host strong electric fields that greatly change the carrier density in adjacent materials, thus tuning their properties in a non-volatile manner. Figure 6(a) shows their basic concept of ferroelectrically controlled spin-to-charge conversion. They switch the polarization direction by applying different gate biases on STO with ferroelectric properties. As a result, the pumped spin current can be converted into positive or negative charge currents under different polarization conditions. Figure 6(b) shows the electric field manipulation of spin-to-charge current conversion where achieved λ_{IEE} is $\pm$ 60 nm. Figure 6(c) shows the normalized charge current produced after applying $\pm$ 200 V voltage pulses, demonstrating non-volatile control of spin-to-charge conversion. It is noteworthy that the polarization direction of ferroelectric STO can be manipulated by an electric field to induce spin current conversion into charge current, and the converted current has characteristics similar to a hysteresis loop under different polarization states. Figure 6(d) illustrates the relationship of ΔI_c with temperature. This non-volatile gate-tunable 2DEGs spin flow conversion into charge flow induced by ferroelectric properties rather than ferromagnetic properties opens a new path for low-power spintronics.

$La_{0.67}Sr_{0.33}MnO_3$ (LSMO) is a strongly correlated half-metallic ferromagnetic-perovskite oxide that can be epitaxially grown on STO due to the small lattice mismatch of ~0.8%. As a result, LSMO is an ideal candidate for exploring efficient spin injection and intrinsic spin-to-charge conversion. Ohya *et al* [22] researched the epitaxial single-crystal heterostructure of LSMO/LAO/STO (figure 7(a)), which can suppress spin scattering and provide an ideal environment for studying intrinsic spin-to-charge conversion. As is shown in figure 7(b), the efficiency of spin-to-charge conversion is enhanced at lower temperatures, with a significant increase to +6.7 nm at 20 K. The efficiency can be further improved by controlling the density and relaxation time of carriers. Band structure calculations reproduce this behavior well and predict that by adjusting the position of the Fermi level near the Lifshitz point [69, 70], the efficiency of spin-to-charge conversion will be further significantly improved. In order to achieve a larger IEE efficiency, a larger α_R, a larger momentum/spin relaxation time (τ) and efficient spin current propagation are required. Recently, Kaneta-Takada *et al* [24] used strongly correlated polar metal $LaTiO_{3+\delta}$ (LTO) layers to carefully cultivate high-quality fully epitaxial LSMO/LTO/STO heterostructures via molecular beam epitaxy (MBE), which is shown in figure 7(c). They demonstrated a large spin-to-charge conversion efficiency using spin pumping ferromagnetic resonance voltage measurements. LTO has a high resistivity ρ,
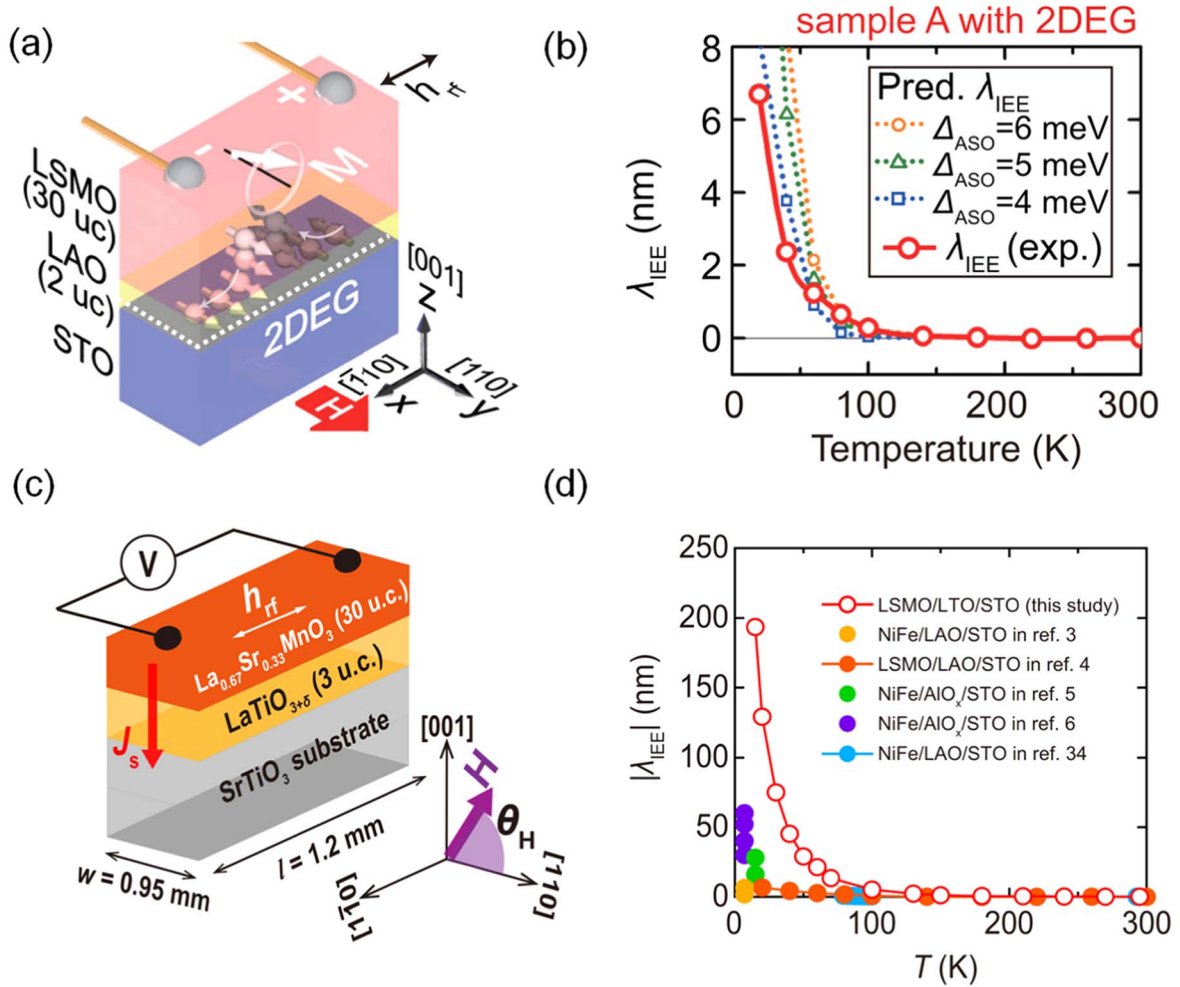
Figure 7. (a) Schematic illustration of the multilayer structure of LSMO/LAO grown on an STO (001) substrate. (b) Temperature dependences of experimental λ_{IEE} and predicted λ_{IEE}. Reproduced from [22]. CC BY 4.0. (c) Schematic structure of the LSMO/LTO/STO sample used for spin pumping measurements. (d) Summary of the temperature dependences of λ_{IEE} in various material systems (The references in the figure are from the original text). Reproduced from [24]. CC BY 4.0.

which can prevent the reduction of two-dimensional electron τ. In addition, the sharpness of the interface in the heterostructures is also thought to substantially increase τ due to the suppression of interface roughness scattering. Apart from that, LTO has excellent lattice matching and metal abundance, so spin current can be effectively propagated in LTO. Therefore, LTO is a suitable material for maximizing τ and spin current propagation, resulting in a larger IEE efficiency. Figure 7(d) shows λ_{IEE} as a function of temperature, as well as data from various STO interfaces with other materials [21, 22, 25, 95, 97]. The large increase in dielectric constant [98] leads to an increase in STO's τ. Therefore, as temperature (T) decreases, λ_{IEE} increases significantly. Notably, Kaneta-Takada *et al* [24] achieved a giant λ_{IEE} of 193.5 nm at 15 K, which is the highest value reported among all materials including spin Hall systems.

3.3. Thermal spin injection

Thermal spin injection is a recently discovered spin current phenomenon that originates from the spin dependence of the Seebeck coefficient, which may offer an innovative way to simplify device integration without the need for electric power, unlike spin pumping by magnetization dynamics. Zhang *et al* [18] successfully obtained 2DEGs by constructing epitaxial heterostructures with ferromagnetic EuO and KTaO$_3$ (figure 8(a)). They found that the 2DEGs at the EuO/KTO interface can directly receive thermally injected spin current from EuO and convert the spin current to charge current via the inverse Edelstein effect of the interface. They used a thermal gradient to efficiently inject spin current into the 2DEG, which is called the spin Seebeck effect. The spin Seebeck effect is zero without a thermal gradient, which means that a temperature difference is required to generate this effect. The spin Seebeck effect also increases with increasing heating power so can be controlled by adjusting the heating power. The potential parasitic effects [99–102] that spin pumping injection may generate, including the dc electromotive forces due to rf-current rectification via anisotropic magnetoresistance effect, planar Hall effect, and anomalous Hall effect, will lead to a misunderstanding of the experimental results [103]. Spin injection takes place in the manner of thermal diffusion of non-equilibrium magnons
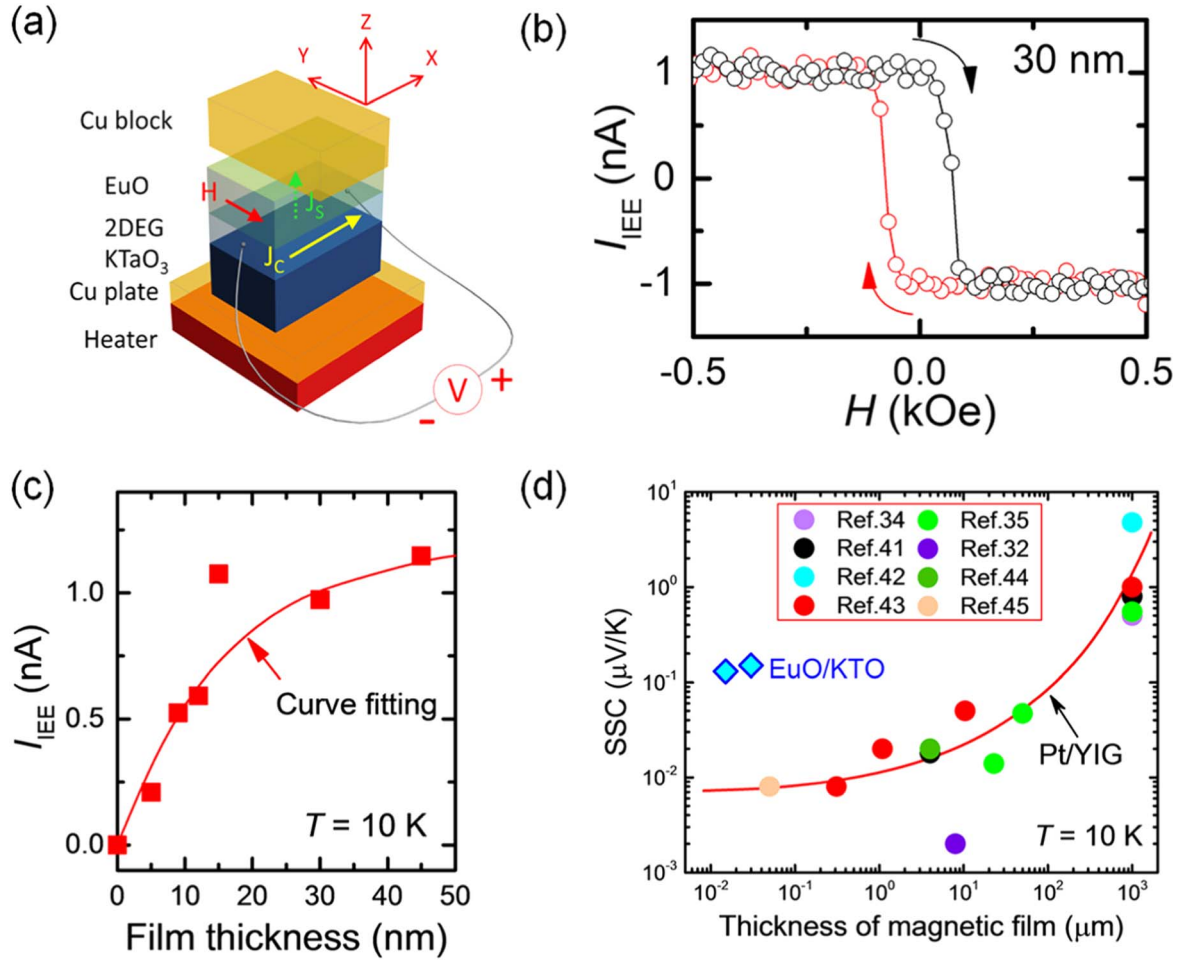
Figure 8. (a) Spin injection via spin Seebeck effect. (b) Magnetic-field dependence of thermoelectric current for the EuO of 30 nm. (c) Converted charge current as a function of the thickness of EuO. (d) Spin Seebeck coefficient as a function of the thickness of magnetic layer for the EuO/KTO (diamonds) and Pt/YIG (solid circles) hybrid structure (The references in the figure are from the original text). Reprinted with permission from [18]. Copyright (2019) American Chemical Society.

rather than electron transmission through EuO. This approach effectively avoids the impedance of oxide insulators to spin currents. Since thermal spin injection is driven by a temperature gradient, it eliminates possible parasitic effects associated with ferromagnetic resonance (FMR). Zhang *et al* [18] conducted a systematic study on samples with varying thicknesses of EuO layers. The I_{IEE}-H measurement curve for a 30 nm thick EuO sample is shown in figure 8(b), and a rectangle-shaped clockwise I_{IEE}–H loop is formed. Notably, there is a non-zero threshold magnetic field that causes the current to reverse due to the coercive field of EuO layer causing magnetization reversal. Thus, the analysis of the I_{IEE}–H measurement results confirmed that the spin-to-charge conversion here has been driven by the spin Seebeck IEE of the 2DEG. As shown in figure 8(c), the thermoelectric current increases with increasing thickness of the EuO layer but not linearly. This is because thicker EuO layers can provide more non-equilibrium magnets, leading to a thermoelectric effect. However, as the film becomes thicker, the contribution from distant magnets from the interface decreases, slowing down the growth of the thermoelectric current. It is difficult to determine the efficiency of spin-to-charge conversion in

thermal spin injection, due to the difficulty of estimating spin current. To measure thermoelectric efficiency, Zhang *et al* [18] defined a spin Seebeck coefficient (SSC) as the electric field generated by unit temperature gradient via the spin Seebeck effect, which allows comparing thermoelectric efficiency of different systems. As shown in figure 8(d), comparing results for EuO/KTO and Pt/YIG heterostructures with the same thickness for magnetic layer (about 50 nm), SSC of the former system is about 19 times larger than that of the latter system, which indicates that EuO/KTO system has much higher thermoelectric conversion efficiency than Pt/YIG system.

4. Charge-to-spin conversion in 2DEGs

Spin current induced by a charge current has been extensively explored to electrically manipulate magnetism and high charge-to-spin conversion efficiency is expected to enable a low power spin–orbit torque (SOT) [104–107] switching mechanism. The efficiency of charge-to-spin conversion can be characterized by many measures.
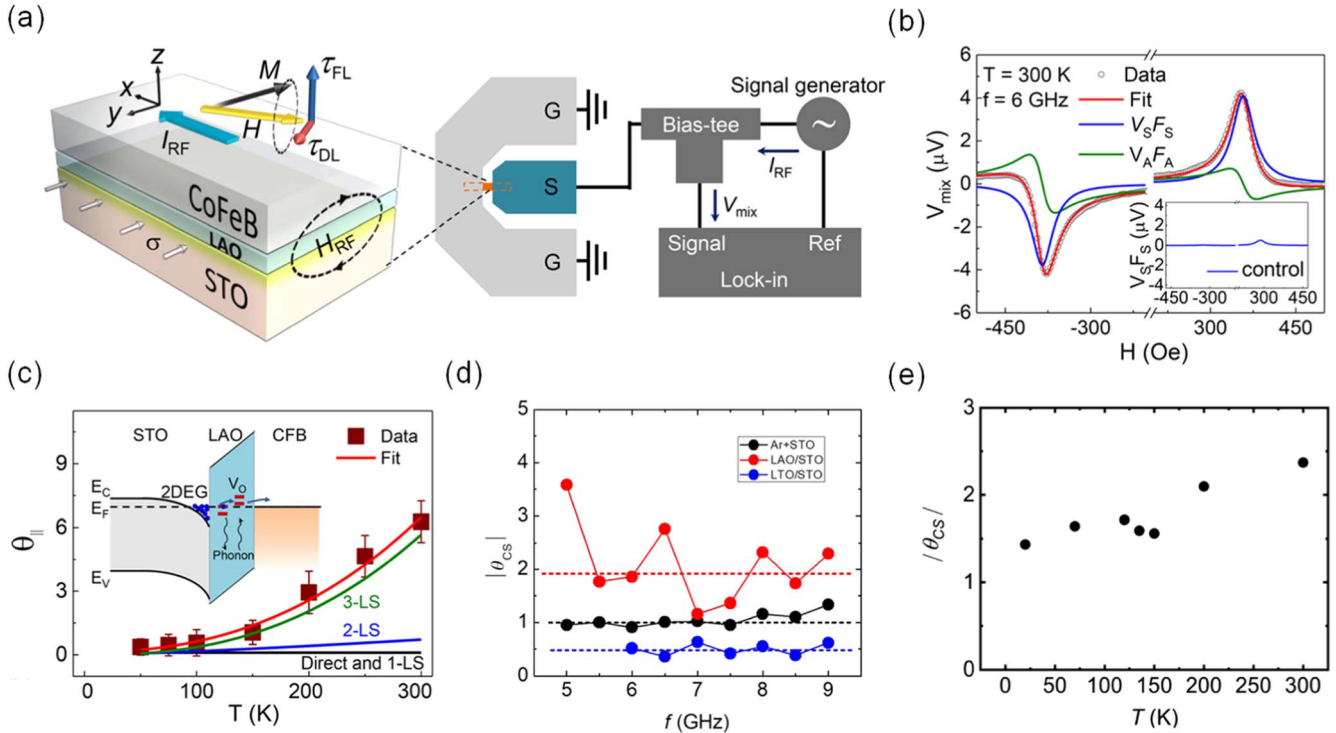
Figure 9. (a) Schematic measurement configuration of ST-FMR for charge-to-spin conversion from CoFeB/LAO/STO devices. (b) Typical ST-FMR signal from the CoFeB/LAO/STO device. (c) SOT efficiency from the CoFeB/LAO/STO device. Reprinted with permission from [26]. Copyright (2017) American Chemical Society. (d) Charge-to-spin conversion efficiency from the device of NiFe/Ar$^+$ etched STO, NiFe/LAO/STO, and NiFe/LTO/STO at different frequencies. Reprinted (figure) with permission from [27], Copyright (2019) by the American Physical Society. (e) Efficiency of charge-to-spin conversion rom the device of NiFe/LTO/STO at different temperatures. Reprinted (figure) with permission from [28], Copyright (2022) by the American Physical Society.

4.1. Spin torque ferromagnetic resonance (ST-FMR)

In 2017, Wang *et al* [26] achieved a significant breakthrough by successfully showcasing the efficient conversion of charge-to-spin in a 2DEG at the LAO/STO interface. This work was accomplished using the spin torque ferromagnetic resonance technique (ST-FMR), as depicted in figure 9(a). By applying radio frequency current (I_{RF}) to the 2DEG, a nonequilibrium spin current was generated via DEE in the CoFeB/LAO/STO heterostructure.

The generated torques make the CoFeB magnetization into precession with the same frequency as I_{RF}. The product of anisotropic magnetoresistance and radio frequency current oscillations generates a mixed voltage V_{mix}, which is detected by a lock-in amplifier (figure 9(b)). The efficiency of charge-to-spin conversion is represented by θ_{CS}:

$$\theta_{CS} = \frac{V_s}{V_a} \frac{e\mu_0 M_0 t_{FM} d}{\hbar} [1 + 4\pi M_{eff}/H_r]^{1/2}, \qquad (4)$$

where the symmetric component V_s is mainly attributed to the damping-like (DL) torque, the antisymmetric component V_a is originated from the field-like (FL) torque and Oersted field, e is the electron charge, $\hbar$ is the reduced Planck constant, $\mu_0 M_0$ is the saturation magnetization of ferromagnetic (FM) layer, t_{FM} is the thickness of FM, d is the thickness of the 2DEGs conducting layer, $4\pi M_{eff}$ is the effective magnetization of FM layer, and H_r is the resonance field, respectively. By calculating the symmetrical component of the voltage V_{mix}, the

efficiency of charge-to-spin (θ_{CS}) is evaluated to be $\sim$6.3 at room temperature (figure 9(c)), which is almost 2 orders of magnitude larger than the spin Hall angles in heavy metals, such as Pt and Ta [97, 108, 109]. Additionally, in contrast to previous SOT devices, the spin source of the 2DEG and the ferromagnetic layer composed of CoFeB are physically separated by the insulating layer of LAO, with no direct contact between them. Remarkably, spin transmission across the LAO overlayer at room temperature is observed, a phenomenon which Wang *et al* [26] attribute to inelastic tunneling facilitated by localized states within the LAO layer. Following this progress, Yang *et al* [27] subsequently reported further achievements in charge-to-spin conversion. Their study showcased effective conversions of charge current to spin current within 2DEGs at various interfaces, including LAO/STO, LaTiO$_3$/STO (LTO/STO), and conducting STO surfaces irradiated by Ar$^+$ ions. Due to the lack of an insulator between the 2DEG and FM layers, the ST-FMR spectrum of a 5-nm-thick NiFe layer on Ar$^+$etched STO shows a larger signal amplitude. According to equation (4), the $4\pi M_{eff}$ represents the contribution of interfacial anisotropy. The interfacial anisotropy of all three types of devices studied is found to be very large. The contribution of interfacial anisotropy for NiFe/Ar$^+$ etched STO is 0.93 T, for NiFe/LAO/STO is 0.92 T, and for NiFe/LTO/ STO is 0.90 T via calculation. In addition, they calculated the charge-to-spin conversion efficiency at different microwave-
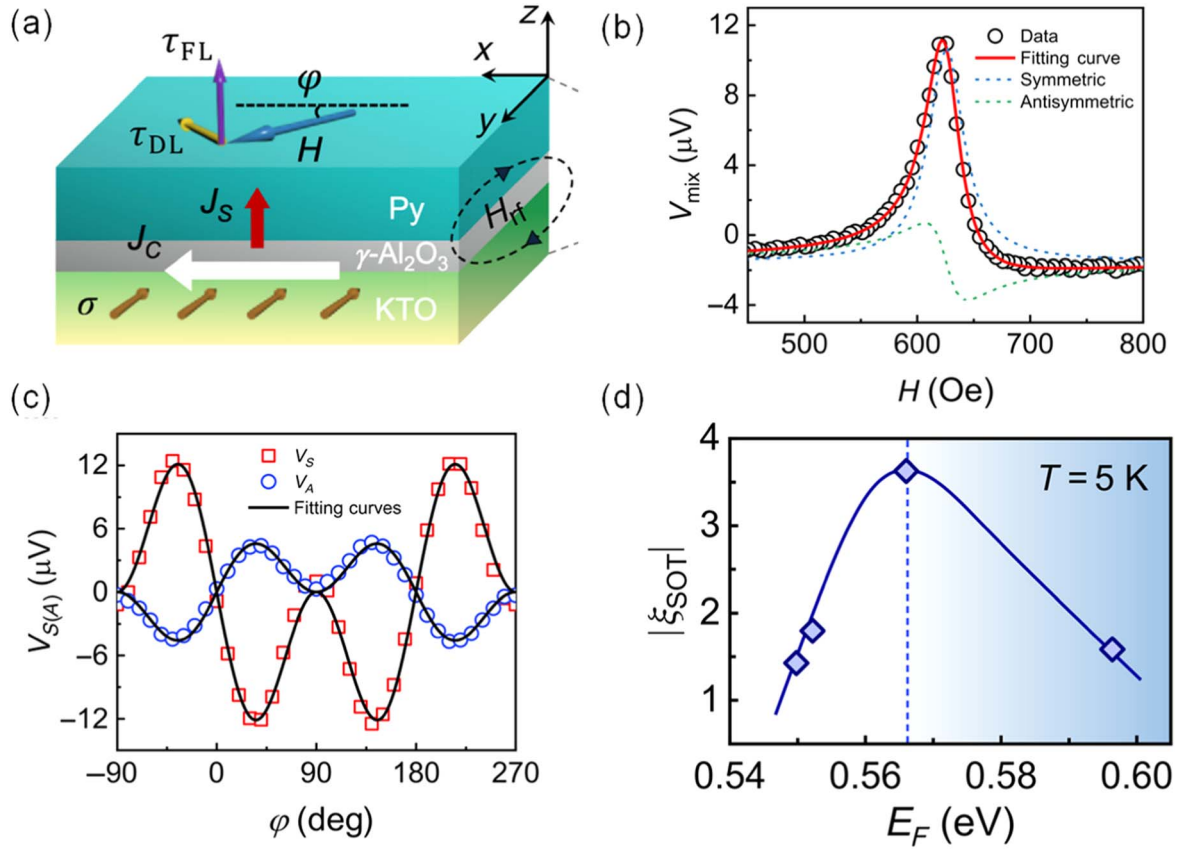
Figure 10. (a) Schematic configuration for Py/γ-Al$_2$O$_3$/KTO devices. (b) Typical ST-FMR signal from the device of Py/γ-Al$_2$O$_3$/KTO. (c) Angular dependence of V_S and V_A. (d) Charge-to-spin conversion efficiency as a function of the Fermi energy. Reprinted (figure) with permission from [112], Copyright (2023) by the American Physical Society.

Table 1. The efficiency of charge-to-spin conversion obtained from ST-FMR measurements.

2DEG	Configuration	Charge-to-spin conversion efficiency ($|\theta_{CS}|$)
LAO/STO	CoFeB/LAO/STO	6.3 at 300 K [26]
Ar$^+$ etched STO	NiFe/Ar$^+$ etched STO	0.9 at 300 K [27]
LAO/STO	NiFe/LAO/STO	1.8 at 300 K [27]
LTO/STO	NiFe/LTO/STO	0.6 and 2.4 at 300 K [27, 28]
γ-Al$_2$O$_3$/KTO	Py/γ-Al$_2$O$_3$/KTO	3.6 at 5 K and 1.1 at 300 K [112]

frequencies of the AC current I_{RF}. At a frequency of 6 GHz, the LAO/STO, LTO/STO, and Ar$^+$ etched STO interfaces exhibit charge-to-spin conversion efficiencies of 1.8, 0.6, and 0.9, respectively. These efficiencies surpass those typically observed in conventional heavy metal systems [109–111] (figure 9(d)). This will enable SrTiO$_3$-based 2DEGs SOT devices for low-power non-volatile memory and logic. Zhang *et al* [28] observed a charge-to-spin conversion efficiency at the LaTiO$_{3+\delta}$/SrTiO$_3$ interface. The charging current flowing along the LTO/STO interface can effectively generate a spin current, producing a SOT in the adjacent NiFe layer, with a maximum conversion efficiency of about 2.4 at room temperature. As shown in figure 9(e), $|\theta_{CS}|$ ranges 1.5–2.4 as temperature varies. This may help to expand the range of SOT-based spintronic applications and demonstrates the great potential of oxide 2DEGs in spintronic applications.

It's worth noting that Zhang *et al* [112] are the only ones to have reported the realization of charge-to-spin conversion through ST-FMR in KTO-based systems, as shown in figures 10(a) and (b). The conversion efficiency as high as approximately 3.6 at 5 K and 1.1 at 300 K are detected for the Py/γ-Al$_2$O$_3$/KTO with a γ-Al$_2$O$_3$ layer of 3 unit cell (u.c.), which are more than an order of magnitude higher than that of Pt (about 0.07 at 300 K). We sort out the efficiency of charge-to-spin conversion obtained from ST-FMR measurements, which is shown in table 1. Moreover, the full angle dependent ST-FMR measurements are carried out as the magnetic field rotates the magnetization direction of the Py layer in the sample plane at room temperature, as is shown in figure 10(c), suggesting that the Rashba effect at the γ-Al$_2$O$_3$/KTO interface is opposite in sign to that for the heavy metal Pt. It is worth noting that a strong dependence of the conversion
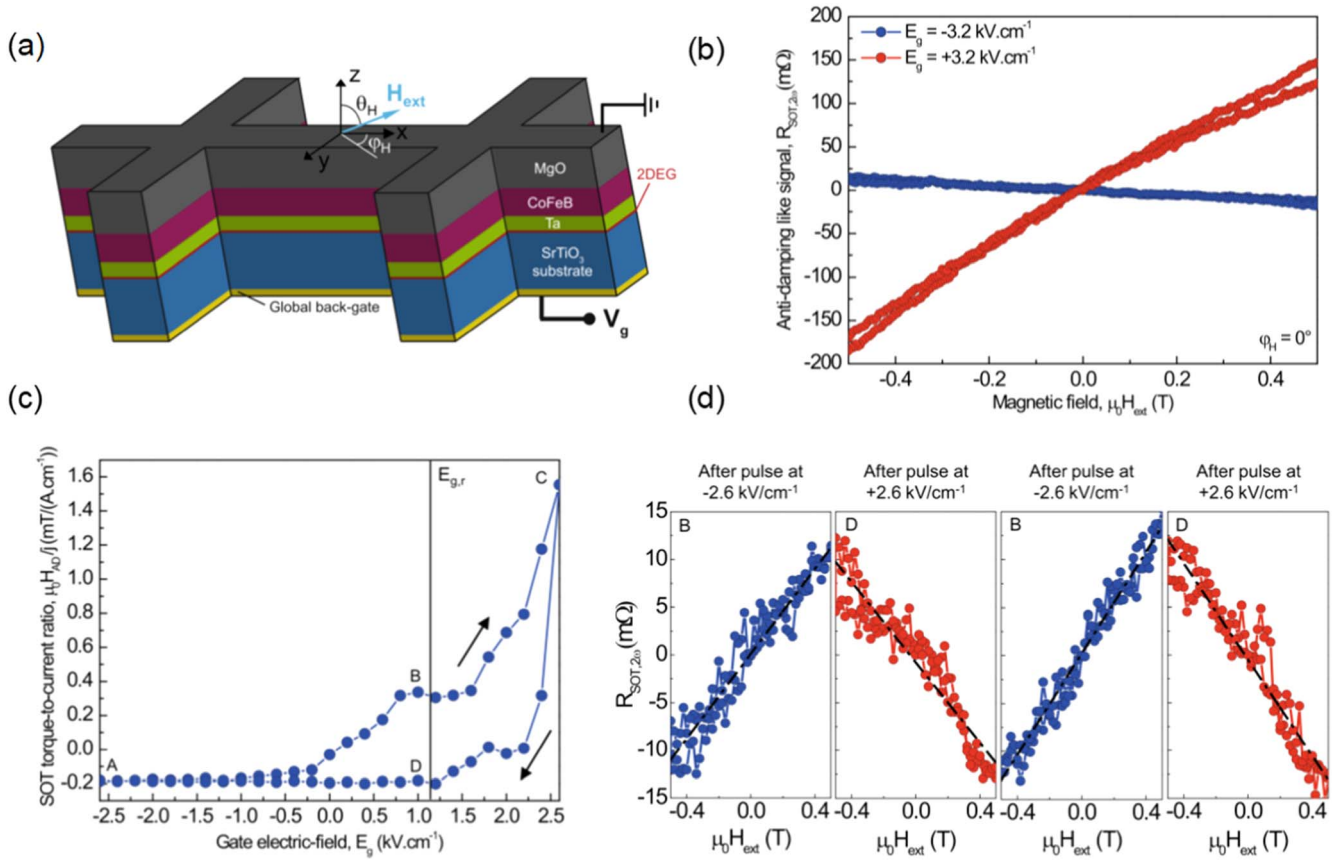
Figure 11. (a) Schematic measurement configuration of second-harmonic Hall for charge-to-spin conversion from MgO/CoFeB/Ta/STO devices. (b) Spin–orbit torques characterization by second-harmonic Hall measurement. (c) Gate electric-field dependence of the spin–orbit torques anti-damping-like effective field $\mu_0 H_{AD}$. (d) Normalized second-harmonic Hall resistance at shifted electrical remanence $E_{g,r}$ after successive application of negative (blue) or positive (red) gate-electric-field pulses of $\pm 2.6\ kV\ cm^{-1}$. Reproduced from [21]. CC BY 4.0.

efficiency on band filling is observed, and the most efficient conversion takes place at the filling level corresponding to Lifshitz transition (figure 10(d)). Theoretical analysis indicates that enhanced spin splitting of the electronic band structure is responsible for efficient conversion.

4.2. Second-harmonic Hall measurement

In addition to using ST-FMR to characterize the efficiency of charge-to-spin conversion, Grezes *et al* [21] recently used harmonic Hall voltage measurements to quantify spin–orbit torque. They achieved non-volatile electric field control of spin–orbit torque (SOT) in MgO/CoFeBa/Ta/STO devices, as shown in figure 11(a). By injecting an AC current of up to 600 μA along the *x*-direction, they induced small oscillations in magnetization near its equilibrium and generated contributions to the Hall resistance of the first and second harmonics. The second harmonic signal provided a sensitive method for measuring the current-induced SOT effective field [113–115]. Figure 11(b) shows the second harmonic Hall resistance under positive and negative gate fields along the *x*-axis, corresponding to anti-damping like torque.

Figure 11(c) shows the measured SOT anti-damping like effective field per linear current density $\mu_0 H_{AD}/j$, as a function of the gate-electric field. The results show a remanent modulation of the SOT-H_{AD} effective field, with inversion of

the H_{AD} sign for opposite maximum gate-electric fields. The dependence shows a hysteresis that is inverted. Thus, the SOT hysteresis can be understood as resulting from both the current redistribution in the stack when varying the 2DEG resistivity, and the variations of the conversion with the 2DEG Fermi level position. Therefore, the ability to manipulate the 2DEG using gate voltage provides degrees of freedom not available in classical ferromagnetic/spin Hall effect bilayers, where the sign and amplitude of SOT under a given current are fixed by the stack structure. SOT can be electrically controlled in a non-volatile manner in both amplitude and sign. Figure 11(d) further demonstrates the dynamic control of the SOT effective field, showing the normalized second harmonic Hall resistance measured at the residual shift after applying gate field pulses, proving the repeatability of the reversal of the SOT torque sign. The experiment was not performed at zero field but at shifted electrical remanence $E_{g,r}$. Their work paves the way for electrically reconfigurable SOT MRAM circuits, SOT oscillators, skyrmion and domain wall-based devices, and magnetic resonance circuits [20, 116].

4.3. Non-reciprocal charge transport

Another way to characterize the conversion of charge flow to spin flow is through the current-induced effect. When a charge current is passed through Rashba 2DEGs, it generates
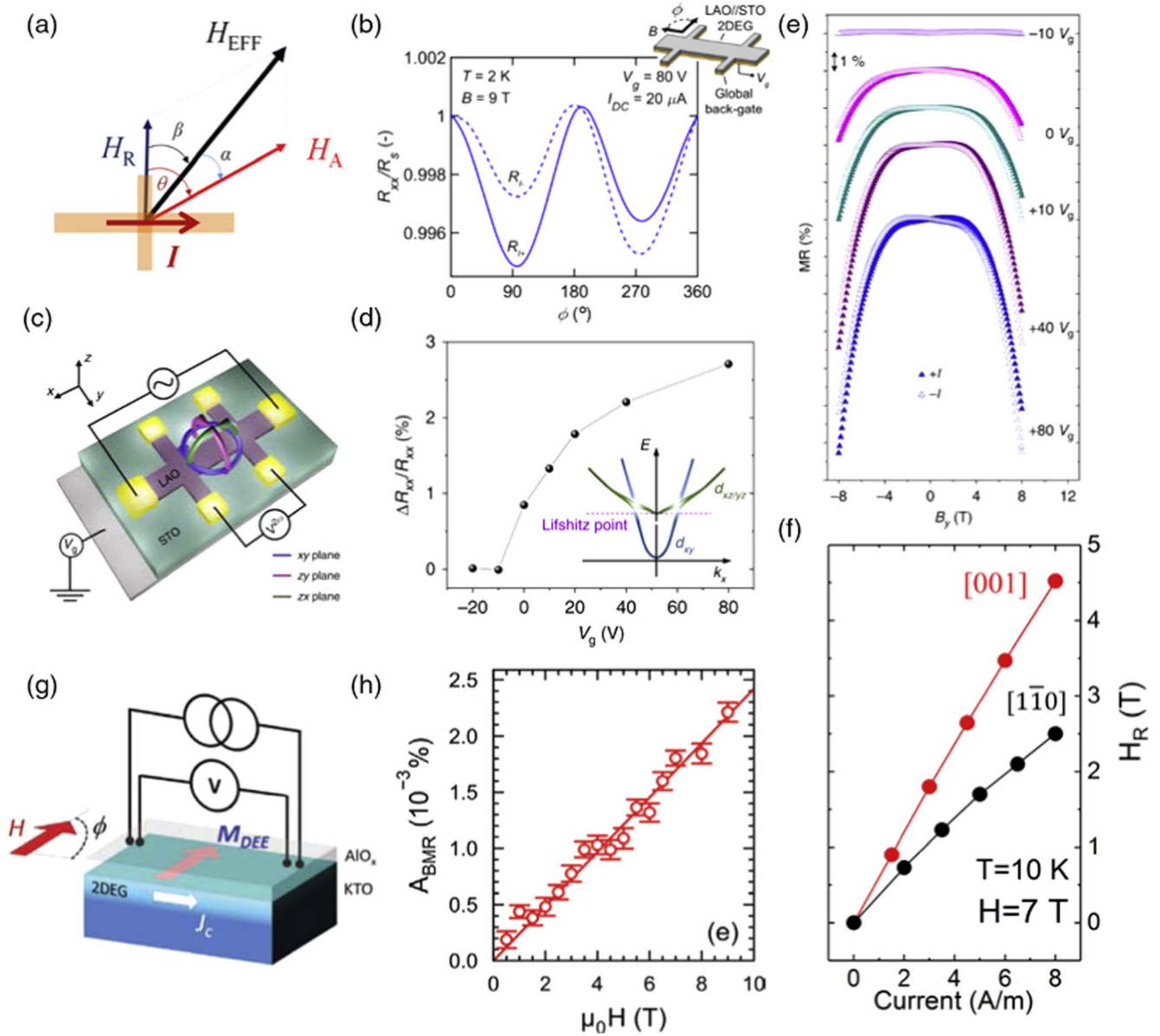
Figure 12. (a) The superposition relationship between Rashba spin–orbit field H_R and applied field H_A. Reprinted from [117], with the permission of AIP Publishing. (b) Measurement of anisotropic magnetoresistance at the LAO/STO interface. Reprinted (figure) with permission from [118], Copyright (2020) by the American Physical Society. (c) Schematic diagram of current effect test. (d) The nonreciprocal resistance $\Delta R_{xx}/R_{xx}$ as a function of gate voltage. The inset displays the sub-band hierarchy of the 2DEG at (001) LAO/STO interface. (e) In-plane MR curves measured for the LAO/STO at various applied gate voltages where $T = 8$ K and $I_x = \pm 30\ \mu$A. Reproduced from [119]. CC BY 4.0. (f) Rashba spin–orbit field H_R fitted for 2DEG based on (110) STO with different orientations. Reprinted (figure) with permission from [120], Copyright (2021) by the American Physical Society. (g) Schematic diagram of current effect at AlO_x/KTO interface. (h) Bilinear magnetoresistance at AlO_x/KTO interface. [17] John Wiley & Sons. © 2021 Wiley-VCH GmbH.

a transverse spin density [17, 65]. In experiments, the current-induced effect is mainly described by analyzing the current-induced Rashba spin–orbit field. However, the Rashba spin–orbit field cannot be directly measured, so it is mainly characterized and fitted by measuring magnetoresistance and anisotropic magnetoresistance to reflect the ability of charge-to-spin conversion. In 2014, Narayanapillai *et al* first proposed a theoretical model of a synthetic magnetic field H_{EFF}, as shown in figure 12(a) [117]. They believe that the root cause of the change in magnetoresistance is the combined action of the current-induced Rashba spin–orbit field H_R

perpendicular to the current and the applied magnetic field H_A. At the same time, they gave a theoretical formula for quantitatively analyzing the Rashba spin–orbit field : $H_{EFF}^2 = H_A^2 + H_R^2 + 2H_A H_R \cos\phi$ and $\alpha = \arctan [\ H_R \sin\phi\ / (H_A + H_R \cos\phi)]$. Through this model, they measured and analyzed the anisotropic magnetoresistance of the LAO/STO interface. It is worth noting that the direction and magnitude of H_R are related to the direction and magnitude of the applied current. Soon after, Vaz *et al* [118] also analyzed the current effect at the LAO/STO interface, as shown in figure 12(b). They measured the anisotropic magnetoresistance under the
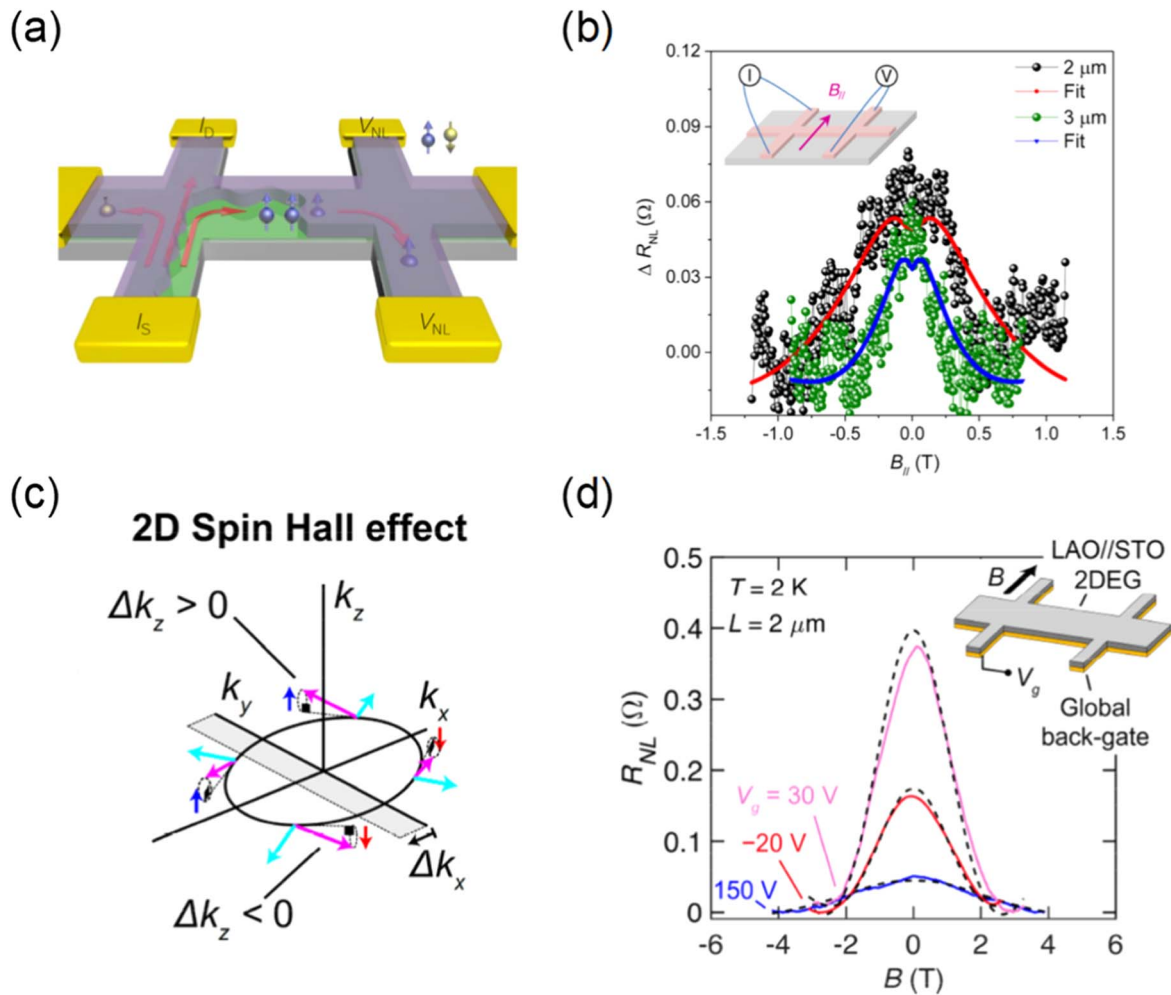
Figure 13. (a) Schematic diagram of 2D Spin Hall effect. (b) Nonlocal voltage measured in the presence of an applied in-plane magnetic field. Reprinted with permission from [121]. Copyright (2017) American Chemical Society. (c) Interpretation of 2D Spin Hall effect. (d) Nonlocal resistance as a function of the applied magnetic field. Reprinted with permission from [123]. Copyright (2020) American Chemical Society.

conditions of $T = 2$ K, $B = 9$ T, $V_g = 80$ V, and observed a large non-reciprocal charge transport. They analyzed the bilinear characteristics of magnetoresistance, that is, A_{BMR} is linearly related to current density and magnetic field. Based on this, Vaz *et al* [118] proposed a new theoretical model for determining Rashba parameters. In addition, Choe *et al* [119] first performed gate voltage regulation of non-reciprocal charge transport at the LAO/STO interface, with the test diagram shown in figure 12(c). Since the Rashba spin–orbit interaction in the LAO/STO conductive interface is gate-controllable, Choe *et al* [119] applied a gate voltage V_g to reflect the non-reciprocal response. As shown in figure 12(e), MR was measured by applying different gate voltages. For each applied gate voltage, magnetoresistance MR was measured in two directions of current $+I_x$ and $-I_x$. The strong asymmetric V_g dependence of the nonreciprocal response can be observed. The ratio of resistance changes $\Delta R_{xx}/R_{xx}$ between $+I_x$ and $-I_x$ is plotted as a function of gate voltage in figure 12(d). When V_g is applied, the sub-band hierarchy along the (001) STO of 2DEG causes significant changes in spin–orbit interaction, leading to the transition of Lifshitz points (figure 12(d) inset). Apart from that, the gate-

controllable spin–orbit interaction can be inferred from the crossover between weak localization and weak anti-localization behavior at low temperatures [13]. Recently, Zhang *et al* [120] studied the strong anisotropic bilinear magnetoresistance of 2DEG based on (110) STO. They found that the bilinear magnetoresistance (BMR) measured along the [001] axis can be 5 times that measured along the [112] axis, explored the close relationship between BMR and current-induced effective Rashba spin–orbit field, and determined an effective Rashba spin–orbit field of up to 4.5 T, which is shown in figure 12(f). This work demonstrates the great potential of anisotropic 2DEG for the exploration of unusual effects. In addition to SrTiO$_3$-based 2DEG, Bibes' group [17] recently reported the direct Edelstein effect in a new interface 2DEG based on perovskite oxide KTaO$_3$, as shown in figure 12(g). 2DEGs are generated by the simple deposition of Al metal onto KTaO$_3$ single crystals, shown to display the DEE through unidirectional magnetoresistance. Figure 12(h) shows the bilinear magnetoresistance at the AlO$_x$/KTO interface, contributing to the exploration of charge-to-spin conversion based on KTO.

4.4. Double Hall bar nonlocal measurements

In contrast to external spin injection [20, 25], Jin *et al* [121] employed the two-dimentional Spin Hall effect (2D-SHE) [122] as a means to generate spin currents in a 2DEG of STO with Rashba spin–orbit coupling, realizing the charge-to-spin conversion. As depicted in figure 13(c), when a charge current (j_c^{inject}) is applied along the x direction, the Fermi contours are displaced by Δk along $-x$ which results in the generation of a transverse spin density oriented along y direction, through the direct Edelstein effect. This spin density can then diffuse and produces a transverse spin current in the material or in adjacent layers. Furthermore, as a result of the displacement of the Fermi contours by Δk, the electrons experience a precession of their spins around the new expected spin direction. This precession causes the tilting of the spins along the $+z$ direction for $k_y > 0$ and the $-z$ direction for $k_y < 0$. As a consequence, a spin current polarized along the z direction is created in the y direction. This is the two-dimentional spin Hall effect.

Within systems featuring pronounced spin–orbit interactions, longitudinal charge currents give rise to transverse spin currents through the mechanism of the spin Hall effect. Oxide heterostructures provide an advantageous platform for the generation of spin-polarized currents via the spin Hall effect, facilitating further investigations into non-local spin diffusion. Jin *et al* bypassed the problem of the low spin injection efficiency at a LAO/STO interface by generating a spin current instead through the inherent spin Hall effect and demonstrate the non-local spin transport [90, 94, 121, 124]. Figure 13(a) illustrates the basic concept of a four-terminal non-local configuration. The SHE facilitates the conversion of locally applied charge current into a transverse spin current, which subsequently diffuses to non-local terminals. Through an analysis of the channel length-dependent Hanle effect observed in a four-terminal non-local device (figure 13(b)), it has been posited that the Spin Hall coefficient (angle) measures at 0.15, while a more dependable spin lifetime of 150 ps is attained at low temperatures.

Trier *et al* [123] took a different approach compared to Jin *et al* [121] in fabricating Hall bar devices. Instead of using electron beam lithography, they utilized pulsed laser deposition to create Hall bar devices with varying channel lengths. Through their experiments, they were able to establish a precise relationship between the non-local spin voltage and the channel length [111]. In their study, they observed the nonlocal resistance as a function of the magnetic field (B) applied along the x-axis. The results depicted in figure 13(d) demonstrate a significant charge-to-spin conversion efficiency, which can be effectively adjusted by an electric field. Remarkably, by manipulating the experimental conditions, such as the electric field, it was possible to tune the Spin Hall coefficient to values ranging from 5% to over 40%.

5. Conclusion

This review mainly introduces the mutual conversion of spin and charge in 2DEG at oxide interfaces. Due to the confinement of electrons in a two-dimensional plane and the breaking of spatial inversion symmetry, there is a large spin–orbit coupling of the 2DEG at the oxide interface compared to traditional semiconductors. In addition, the strength of Rashba spin–orbit coupling can be modulated by external electric fields, allowing control of electron spin. Currently, research on spin-charge interconversion in oxide 2DEGs is mainly based on STO-based and KTO-based 2DEGs. The conversion of spin current to charge current is mainly carried out through the inverse Edelstein effect. There are three main ways to inject spin current: electrical spin injection, spin pumping injection and thermal spin injection. The electrical injection method is simple, but it is difficult to detect electrical signals. Spin pumping is the most widely used method for injecting spin current with a range of advantages, such as efficient spin-current transport and strong controllability. Thermal spin injection may provide an innovative way to simplify device integration without electricity and eliminate the potential parasitic effect of spin pumping while it's difficult to determine the efficiency of spin-to-charge conversion via thermal spin injection. There are four main research methods for charge-to-spin conversion: ST-FMR, second-harmonic Hall measurement, non-reciprocal charge transport and double Hall bar nonlocal measurements. Among them, ST-FMR is the only method that can directly derive the charge-to-spin conversion efficiency. DL and FL moments can be analyzed quantitatively by second-harmonic Hall measurement. Non-reciprocal charge transport is the simplest way to measure the efficiency of conversing charge current to spin current which can be intuitively reflected by changes in resistance and double Hall bar nonlocal measurements detect the charge-to-spin conversion by the spin Hall effect rather than the Edelstein effect.

Overall, utilizing the high conversion efficiency of charge to spin for 2DEGs at the oxide interfaces, it is anticipated that the flipping of magnetic moments in ferromagnetic layers can be achieved. This enables the implementation of SOT in structures comprising ferromagnetic layers and 2DEG heterojunctions, thereby facilitating the development of novel magnetic storage devices. The high conversion efficiency of spin to charge makes oxide 2DEGs suitable for the spin–orbit (SO) unit in mgnetoelectric spin–orbit (MESO) [125] logic devices for information read-out. However, there exists an insulating oxide layer between the ferromagnetic layer and the conducting 2DEG. This layer hampers the transport of spin and charge currents, which maybe a problem for impeding the realization of functionalities in magnetic storage devices. It is expected to improve higher transmission efficiency and spin-charge interconversion efficiency for 2DEGs at the oxide interfaces for applications in ultra-low power spintronics devices. We sincerely hope that this article will provide a clear overview of spin-charge interconversion of 2DEGs at the oxide interfaces and inspire more investigations on this promising research field.

Data availability statement

All data that support the findings of this study are included within the article (and any supplementary files).

Conflict of interest

The authors declare no conflict of interest.

ORCID iDs

Dongyao Zheng ⬤ https://orcid.org/0009-0007-0228-1773
Hui Zhang ⬤ https://orcid.org/0000-0003-1238-8770
Fengxia Hu ⬤ https://orcid.org/0000-0003-0383-0213
Jirong Sun ⬤ https://orcid.org/0000-0003-4531-4794
Weisheng Zhao ⬤ https://orcid.org/0000-0001-8088-0404

References

[1] Ohtomo A and Hwang H Y 2004 A high-mobility electron gas at the LaAlO$_3$/SrTiO$_3$ heterointerface *Nature* **427** 423–6

[2] Zhang M, Du K, Ren T, Tian H, Zhang Z, Hwang H Y and Xie Y 2019 A termination-insensitive and robust electron gas at the heterointerface of two complex oxides *Nat. Commun.* **10** 4026

[3] Xu P *et al* 2017 Reversible Formation of 2D Electron Gas at the LaFeO$_3$/SrTiO$_3$ Interface via control of oxygen vacancies *Adv. Mater.* **29** 1604447

[4] Niu W, Gan Y, Zhang Y, Christensen D V, Wang X, Xu Y, Zhang R, Pryds N and Chen Y 2017 Suppressed carrier density for the patterned high mobility two-dimensional electron gas at c-Al$_2$O$_3$/SrTiO$_3$ heterointerfaces *Appl. Phys. Lett.*

[5] Chen Y, Pryds N, Kleibeuker J E, Koster G, Sun J, Stamate E, Shen B, Rijnders G and Linderoth S 2011 Metallic and insulating interfaces of amorphous SrTiO$_3$-Based oxide heterostructures *Nano Lett.* **11** 3774–8

[6] Niu W *et al* 2019 Electrolyte gate controlled metal-insulator transitions of the CaZrO$_3$/SrTiO$_3$ heterointerface *Appl. Phys. Lett.* **115** 061601

[7] Han K *et al* 2019 Erasable and recreatable two-dimensional electron gas at the heterointerface of SrTiO$_3$ and a water-dissolvable overlayer *Sci. Adv.* **5** eaaw7286

[8] Herranz G *et al* 2007 High mobility in LaAlO$_3$/SrTiO$_3$ heterostructures: origin, dimensionality, and perspectives *Phys. Rev. Lett.* **98** 216803

[9] Brinkman A, Huijben M, Van Zalk M, Huijben J, Zeitler U, Maan J C, Van Der Wiel W G, Rijnders G, Blank D H A and Hilgenkamp H 2007 Magnetic effects at the interface between non-magnetic oxides *Nat. Mater.* **6** 493–6

[10] Li L, Richter C, Mannhart J and Ashoori R C 2011 Coexistence of magnetic order and two-dimensional superconductivity at LaAlO$_3$/SrTiO$_3$ interfaces *Nat. Phys.* **7** 762–6

[11] Reyren N *et al* 2007 Superconducting interfaces between insulating oxides *Science* **317** 1196–9

[12] Dikin D A, Mehta M, Bark C W, Folkman C M, Eom C B and Chandrasekhar V 2011 Coexistence of superconductivity and ferromagnetism in two dimensions *Phys. Rev. Lett.* **107** 056802

[13] Caviglia A D, Gabay M, Gariglio S, Reyren N, Cancellieri C and Triscone J-M 2010 Tunable rashba spin–orbit interaction at oxide interfaces *Phys. Rev. Lett.* **104** 126803

[14] Niu W *et al* 2017 Giant Tunability of the two-dimensional electron gas at the interface of γ-Al$_2$O$_3$/SrTiO$_3$ *Nano Lett.* **17** 6878–85

[15] Diez M, Monteiro A M R V L, Mattoni G, Cobanera E, Hyart T, Mulazimoglu E, Bovenzi N, Beenakker C W J and Caviglia A D 2015 Giant negative magnetoresistance driven by spin–orbit coupling at the LaAlO$_3$/SrTiO$_3$ Interface *Phys. Rev. Lett.* **115** 016803

[16] Ben Shalom M, Sachs M, Rakhmilevitch D, Palevski A and Dagan Y 2010 Tuning spin–orbit coupling and Superconductivity at the SrTiO$_3$/LaAlO$_3$ Interface: a Magnetotransport Study *Phys. Rev. Lett.* **104** 126802

[17] Vicente-Arche L M *et al* 2021 Spin–charge interconversion in KTaO$_3$ 2D electron gases *Adv. Mater.* **33** 2102102

[18] Zhang H *et al* 2019 Thermal spin injection and inverse edelstein effect of the two-dimensional electron gas at EuO–KTaO$_3$ interfaces *Nano Lett.* **19** 1605–12

[19] Tebano A, Fabbri E, Pergolesi D, Balestrino G and Traversa E 2012 Room-temperature giant persistent photoconductivity in SrTiO$_3$/LaAlO$_3$ heterostructures *ACS Nano* **6** 1278–83

[20] Lesne E *et al* 2016 Highly efficient and tunable spin-to-charge conversion through Rashba coupling at oxide interfaces *Nat. Mater.* **15** 1261–6

[21] Grezes C *et al* 2023 Non-volatile electric control of spin–orbit torques in an oxide two-dimensional electron gas *Nat. Commun.* **14** 2590

[22] Ohya S, Araki D, Anh L D, Kaneta S, Seki M, Tabata H and Tanaka M 2020 Efficient intrinsic spin-to-charge current conversion in an all-epitaxial single-crystal perovskite-oxide heterostructure of La$_{0.67}$Sr$_{0.33}$MnO$_3$/LaAlO$_3$/SrTiO$_3$ *Phys. Rev. Res.* **2** 012014

[23] Song Q, Zhang H, Su T, Yuan W, Chen Y, Xing W, Shi J, Sun J and Han W 2017 Observation of inverse Edelstein effect in Rashba-split 2DEG between SrTiO$_3$ and LaAlO$_3$ at room temperature *Sci. Adv.* **3** e1602312

[24] Kaneta-Takada S *et al* 2022 Giant spin-to-charge conversion at an all-epitaxial single-crystal-oxide Rashba interface with a strongly correlated metal interlayer *Nat. Commun.* **13** 5631

[25] Vaz D C *et al* 2019 Mapping spin–charge conversion to the band structure in a topological oxide two-dimensional electron gas *Nat. Mater.* **18** 1187–93

[26] Wang Y, Ramaswamy R, Motapothula M, Narayanapillai K, Zhu D, Yu J, Venkatesan T and Yang H 2017 Room-temperature giant charge-to-spin conversion at the SrTiO$_3$–LaAlO$_3$ oxide interface *Nano Lett.* **17** 7659–64

[27] Yang H, Zhang B, Zhang X, Yan X, Cai W, Zhao Y, Sun J, Wang K L, Zhu D and Zhao W 2019 Giant charge-to-spin conversion efficiency in SrTiO$_3$-based electron gas interface *Phys. Rev. Appl.* **12** 034004

[28] Zhang J *et al* 2022 Giant efficiency for charge-to-spin conversion via the electron gas at the LaTiO$_{3+\delta}$/SrTiO$_3$ interface *Phys. Rev.* B **105** 195110

[29] Sánchez J C R, Vila L, Desfonds G, Gambarelli S, Attané J P, De Teresa J M, Magén C and Fert A 2013 Spin-to-charge conversion using Rashba coupling at the interface between non-magnetic materials *Nat. Commun.* **4** 2944

[30] Isasa M *et al* 2016 Origin of inverse Rashba-Edelstein effect detected at the Cu/Bi interface using lateral spin valves *Phys. Rev.* B **93** 014420

[31] Karube S, Kondou K and Otani Y 2016 Experimental observation of spin-to-charge current conversion at non-magnetic metal/Bi$_2$O$_3$ interfaces *Appl. Phys. Express* **9** 033001

[32] Kim J, Chen Y-T, Karube S, Takahashi S, Kondou K, Tatara G and Otani Y 2017 Evaluation of bulk-interface contributions to Edelstein magnetoresistance at metal/oxide interfaces *Phys. Rev.* B **96** 140409

[33] Zhang S and Fert A 2016 Conversion between spin and charge currents with topological insulators *Phys. Rev.* B **94** 184423

[34] Pesin D and MacDonald A H 2012 Spintronics and pseudospintronics in graphene and topological insulators *Nat. Mater.* **11** 409–16

[35] Steinberg H, Laloë J-B, Fatemi V, Moodera J S and Jarillo-Herrero P 2011 Electrically tunable surface-to-bulk coherent coupling in topological insulator thin films *Phys. Rev.* B **84** 233101

[36] Wang Haiyu *et al* 2023 Room temperature energy-efficient spin-orbit torque switching in two-dimensional van der Waals Fe$_3$GeTe$_2$ induced by topological insulators *Nature Communications* **14** 5173

[37] Xiao D, Liu G-B, Feng W, Xu X and Yao W 2012 Coupled spin and valley physics in monolayers of MoS$_2$ and other group-VI dichalcogenides *Phys. Rev. Lett.* **108** 196802

[38] Chen H, Niu Q and MacDonald A H 2014 Anomalous Hall effect arising from noncollinear antiferromagnetism *Phys. Rev. Lett.* **112** 017205

[39] Li X, Xu L, Ding L, Wang J, Shen M, Lu X, Zhu Z and Behnia K 2017 Anomalous nernst and righi-leduc effects in Mn$_3$Sn: berry curvature and entropy flow *Phys. Rev. Lett.* **119** 056601

[40] Varignon J, Vila L, Barthélémy A and Bibes M 2018 A new spin for oxide interfaces *Nat. Phys.* **14** 322–5

[41] Manchon A, Koo H C, Nitta J, Frolov S M and Duine R A 2015 New perspectives for Rashba spin–orbit coupling *Nat. Mater.* **14** 871–82

[42] Seibold G, Caprara S, Grilli M and Raimondi R 2017 Theory of the spin galvanic effect at oxide interfaces *Phys. Rev. Lett.* **119** 256801

[43] Rojas-Sánchez J-C *et al* 2016 Spin to charge conversion at room temperature by spin pumping into a new type of topological insulator: α-Sn films *Phys. Rev. Lett.* **116** 096602

[44] Khalsa G and MacDonald A H 2012 Theory of the SrTiO$_3$ surface state two-dimensional electron gas *Phys. Rev.* B **86** 125121

[45] King P D C, McKeown Walker S, Tamai A, De La Torre A, Eknapakul T, Buaphet P, Mo S-K, Meevasana W, Bahramy M S and Baumberger F 2014 Quasiparticle dynamics and spin–orbital texture of the SrTiO$_3$ two-dimensional electron gas *Nat. Commun.* **5** 3414

[46] Meevasana W, King P D C, He R H, Mo S-K, Hashimoto M, Tamai A, Songsiriritthigul P, Baumberger F and Shen Z-X 2011 Creation and control of a two-dimensional electron liquid at the bare SrTiO$_3$ surface *Nat. Mater.* **10** 114–8

[47] Bruno F Y, McKeown Walker S, Riccò S, La Torre A, Wang Z, Tamai A, Kim T K, Hoesch M, Bahramy M S and Baumberger F 2019 Band structure and spin–orbital texture of the (111)-KTaO$_3$ 2D electron gas *Adv. Electron. Mater.* **5** 1800860

[48] Qi S, Zhang H, Zhang J, Gan Y, Chen X, Shen B, Chen Y, Chen Y and Sun J 2022 Large optical tunability of 5d 2D electron gas at the spinel/Perovskite γ-Al$_2$O$_3$/KTaO$_3$ heterointerface *Adv. Mater. Interfaces* **9** 2200103

[49] Gan Y, Zhang Y, Christensen D V, Pryds N and Chen Y 2019 Gate-tunable Rashba spin–orbit coupling and spin polarization at diluted oxide interfaces *Phys. Rev.* B **100** 125134

[50] Zhang H *et al* 2017 Highly mobile two-dimensional electron gases with a strong gating effect at the amorphous LaAlO$_3$/KTaO$_3$ interface *ACS Appl. Mater. Interfaces* **9** 36456–61

[51] Zhang H R *et al* 2017 Magnetic two-dimensional electron gas at the manganite-buffered LaAlO$_3$/SrTiO$_3$ interface *Phys. Rev.* B **96** 195167

[52] Zhang H *et al* 2019 Unusual electric and optical tuning of KTaO$_3$-based two-dimensional electron gases with 5d orbitals *ACS Nano* **13** 609–15

[53] Edelstein V M 1990 Spin polarization of conduction electrons induced by electric current in two-dimensional asymmetric electron systems *Solid State Commun.* **73** 233–5

[54] Varotto S *et al* 2022 Direct visualization of Rashba-split bands and spin/orbital-charge interconversion at KTaO$_3$ interfaces *Nat. Commun.* **13** 6165

[55] Gan Y *et al* 2023 Light-induced giant Rashba spin–orbit coupling at superconducting KTaO$_3$ (110) heterointerfaces *Adv. Mater.* **35** 2300582

[56] Kumar N, Wadehra N, Tomar R, Shama, Kumar S, Singh Y, Dattagupta S and Chakraverty S 2021 Observation of shubnikov–de Haas oscillations, planar hall effect, and anisotropic magnetoresistance at the conducting interface of EuO-KTaO$_3$ *Adv. Quantum Technol.* **4** 2000081

[57] Chen G *et al* 2020 Promoted oxygen reduction kinetics on nitrogen-doped hierarchically porous carbon by engineering proton-feeding centers *Energy Environ. Sci.* **13** 2849–55

[58] Singh G, Jouan A, Hurand S, Feuillet-Palma C, Kumar P, Dogra A, Budhani R, Lesueur J and Bergeal N 2017 Effect of disorder on superconductivity and Rashba spin–orbit coupling in LaAlO$_3$/SrTiO$_3$ interfaces *Phys. Rev.* B **96** 024509

[59] Koga T, Nitta J, Akazaki T and Takayanagi H 2002 Rashba spin–orbit coupling probed by the weak antilocalization analysis in InAlAs/InGaAs/InAlAs quantum wells as a function of quantum well asymmetry *Phys. Rev. Lett.* **89** 046801

[60] Takasuna S, Shiogai J, Matsuzaka S, Kohda M, Oyama Y and Nitta J 2017 Weak antilocalization induced by Rashba spin–orbit interaction in layered III-VI compound semiconductor GaSe thin films *Phys. Rev.* B **96** 161303

[61] Nitta J, Akazaki T, Takayanagi H and Enoki T 1997 Gate Control of spin–orbit Interaction in an Inverted In$_{0.53}$Ga$_{0.47}$As/In$_{0.52}$Al$_{0.48}$As Heterostructure *Phys. Rev. Lett.* **78** 1335–8

[62] Schmult S, Manfra M J, Punnoose A, Sergent A M, Baldwin K W and Molnar R J 2006 Large Bychkov–Rashba spin–orbit coupling in high-mobility GaN/Al$_x$Ga$_{1-x}$N heterostructures *Phys. Rev.* B **74** 033302

[63] Lei Z, Cheah E, Rubi K, Bal M E, Adam C, Schott R, Zeitler U, Wegscheider W, Ihn T and Ensslin K 2022 High-quality two-dimensional electron gas in undoped InSb quantum wells *Phys. Rev. Res.* **4** 013039

[64] Koo H C, Kwon J H, Eom J, Chang J, Han S H and Johnson M 2009 Control of spin precession in a spin-injected field effect transistor *Science* **325** 1515–8

[65] Niu W, Wang X, Xu Y and Zhang R 2021 Recent advances on spin-polarized two-dimensional electron gases at oxide interfaces *ACS Appl. Electron. Mater.* **3** 128–44

[66] Shen K, Vignale G and Raimondi R 2014 Microscopic theory of the inverse edelstein effect *Phys. Rev. Lett.* **112** 096601

[67] Zhang Y *et al* 2023 Ferrimagnets for spintronic devices: from materials to applications *Appl. Phys. Rev.* **10** 011301

[68] Zhong Z, Tóth A and Held K 2013 Theory of spin–orbit coupling at LaAlO$_3$/SrTiO$_3$ interfaces and SrTiO$_3$ surfaces *Phys. Rev.* B **87** 161102

[69] Nakagawa N, Hwang H Y and Muller D A 2006 Why some interfaces cannot be sharp *Nat. Mater.* **5** 204–9

[70] Caviglia A D, Gariglio S, Reyren N, Jaccard D, Schneider T, Gabay M, Thiel S, Hammerl G, Mannhart J and Triscone J-M 2008 Electric field control of the LaAlO$_3$/SrTiO$_3$ interface ground state *Nature* **456** 624–7

[71] Joshua A, Pecker S, Ruhman J, Altman E and Ilani S 2012 A universal critical density underlying the physics of electrons at the LaAlO$_3$/SrTiO$_3$ interface *Nat. Commun.* **3** 1129

[72] Santander-Syro A F *et al* 2011 Two-dimensional electron gas with universal subbands at the surface of SrTiO$_3$ *Nature* **469** 189–93

[73] McKeown Walker S, Boselli M, Martínez E A, Gariglio S, Bruno F Y and Baumberger F 2022 A Laser-ARPES View of the 2D Electron Systems at LaAlO$_3$/SrTiO$_3$ and Al/SrTiO$_3$ Interfaces *Adv. Electron. Mater.* **8** 2101376

[74] Uwe H and Sakudo T 1983 Raman scattering in semiconducting KTaO$_3$ and SrTiO$_3$ *Ferroelectrics* **52** 205–10

[75] Uwe H, Sakudo T and Yamaguchi H 1985 Interband electronic Raman scattering in SrTiO$_3$ *Jpn. J. Appl. Phys.* **24** 519–21

[76] Kohda M, Bergsten T and Nitta J 2008 Manipulating spin–orbit interaction in semiconductors *J. Phys. Soc. Jpn.* **77** 031008

[77] King P D C *et al* 2012 Subband structure of a two-dimensional electron gas formed at the polar surface of the strong spin–orbit perovskite KTaO$_3$ *Phys. Rev. Lett.* **108** 117602

[78] Zhang H *et al* 2018 High-mobility spin-polarized two-dimensional electron gases at EuO/KTaO$_3$ interfaces *Phys. Rev. Lett.* **121** 116803

[79] Thiel S, Hammerl G, Schmehl A, Schneider C W and Mannhart J 2006 Tunable quasi-two-dimensional electron gases in oxide heterostructures *Science* **313** 1942–5

[80] Bell C, Harashima S, Kozuka Y, Kim M, Kim B G, Hikita Y and Hwang H Y 2009 Dominant mobility modulation by the electric field effect at the LaAlO$_3$/SrTiO$_3$ interface *Phys. Rev. Lett.* **103** 226802

[81] Herranz G *et al* 2015 Engineering two-dimensional superconductivity and Rashba spin–orbit coupling in LaAlO$_3$/SrTiO$_3$ quantum wells by selective orbital occupancy *Nat. Commun.* **6** 6028

[82] Gopinadhan K, Annadi A, Kim Y, Srivastava A, Kumar B, Chen J, Coey J M D, Ariando and Venkatesan T 2015 Gate tunable in- and out-of-plane spin–orbit coupling and spin-splitting anisotropy at LaAlO$_3$/SrTiO$_3$(110) interface *Adv. Electron. Mater.* **1** 1500114

[83] Veit M J, Arras R, Ramshaw B J, Pentcheva R and Suzuki Y 2018 Nonzero Berry phase in quantum oscillations from giant Rashba-type spin splitting in LaTiO$_3$/SrTiO$_3$ heterostructures *Nat. Commun.* **9** 1458

[84] Liang H, Cheng L, Wei L, Luo Z, Yu G, Zeng C and Zhang Z 2015 Nonmonotonically tunable Rashba spin–orbit coupling by multiple-band filling control in SrTiO$_3$-based interfacial d-electron gases *Phys. Rev.* B **92** 075309

[85] Bisri S Z, Shimizu S, Nakano M and Iwasa Y 2017 Endeavor of iontronics: from fundamentals to applications of ion-controlled electronics *Adv. Mater.* **29** 1607054

[86] Lu N *et al* 2017 Electric-field control of tri-state phase transformation with a selective dual-ion switch *Nature* **546** 124–8

[87] Zeng S *et al* 2016 Liquid-gated high mobility and quantum oscillation of the two-dimensional electron gas at an oxide interface *ACS Nano* **10** 4532–7

[88] Trier F, Noël P, Kim J-V, Attané J-P, Vila L and Bibes M 2021 Oxide spin-orbitronics: spin–charge interconversion and topological spin textures *Nat. Rev. Mater.* **7** 258–74

[89] Nomura A, Tashiro T, Nakayama H and Ando K 2015 Temperature dependence of inverse Rashba–Edelstein effect at metallic interface *Appl. Phys. Lett.* **106** 212403

[90] Reyren N, Bibes M, Lesne E, George J-M, Deranlot C, Collin S, Barthélémy A and Jaffrès H 2012 Gate-controlled spin injection at LaAlO$_3$/SrTiO$_3$ interfaces *Phys. Rev. Lett.* **108** 186802

[91] Dash S P, Sharma S, Le Breton J C, Peiro J, Jaffrès H, George J-M, Lemaître A and Jansen R 2011 Spin precession and inverted Hanle effect in a semiconductor near a finite-roughness ferromagnetic interface *Phys. Rev.* B **84** 054410

[92] Ando Y *et al* 2011 Electric-field control of spin accumulation signals in silicon at room temperature *Appl. Phys. Lett.* **99** 132511

[93] Fert A and Jaffrès H 2001 Conditions for efficient spin injection from a ferromagnetic metal into a semiconductor *Phys. Rev.* B **64** 184420

[94] Inoue H, Swartz A G, Harmon N J, Tachikawa T, Hikita Y, Flatté M E and Hwang H Y 2015 Origin of the magnetoresistance in oxide tunnel junctions determined through electric polarization control of the interface *Phys. Rev. X* **5** 041023

[95] Chauleau J-Y, Boselli M, Gariglio S, Weil R, De Loubens G, Triscone J-M and Viret M 2016 Efficient spin-to-charge conversion in the 2D electron liquid at the LAO/STO interface *EPL Europhys. Lett.* **116** 17006

[96] Manipatruni S, Nikonov D E and Young I A 2018 Beyond CMOS computing with spin and polarization *Nat. Phys.* **14** 338–43

[97] Jin K X, Lin W, Luo B C and Wu T 2015 Photoinduced modulation and relaxation characteristics in LaAlO$_3$/SrTiO$_3$ heterointerface *Sci. Rep.* **5** 8778

[98] Müller K A and Burkard H 1979 SrTiO$_3$: An intrinsic quantum paraelectric below 4 K *Phys. Rev.* B **19** 3593–602

[99] Egan W G and Juretschke H J 1963 DC detection of ferromagnetic resonance in thin nickel films *J. Appl. Phys.* **34** 1477–84

[100] Iguchi R and Saitoh E 2017 Measurement of spin pumping voltage separated from extrinsic microwave effects *J. Phys. Soc. Jpn.* **86** 011003

[101] Harder M, Gui Y and Hu C-M 2016 Electrical detection of magnetization dynamics via spin rectification effects *Phys. Rep.* **661** 1–59

[102] Keller S, Greser J, Schweizer M R, Conca A, Lauer V, Dubs C, Hillebrands B and Papaioannou E T 2017 Relative weight of the inverse spin-Hall and spin-rectification effects for metallic polycrystalline Py/Pt, epitaxial Fe/Pt, and insulating YIG/Pt bilayers: Angular dependent spin pumping measurements *Phys. Rev.* B **96** 024437

[103] Yue D, Lin W, Li J, Jin X and Chien C L 2018 Spin-to-charge conversion in Bi films and Bi/Ag bilayers *Phys. Rev. Lett.* **121** 037201

[104] Guo Z, Yin J, Bai Y, Zhu D, Shi K, Wang G, Cao K and Zhao W 2021 Spintronics for Energy- Efficient Computing: An Overview and Outlook *Proceedings of the IEEE* **109** 1398–417

[105] Du A *et al* 2023 Electrical manipulation and detection of antiferromagnetism in magnetic tunnel junctions *Nature Electronics* **6** 425–33

[106] Peng S *et al* 2020 Exchange bias switching in an antiferromagnet/ferromagnet bilayer driven by spin–orbit torque *Nature Electronics* **3** 757–64

[107] Xiong D *et al* 2022 Antiferromagnetic spintronics: An overview and outlook *Fundamental Research* **2** 522–34

[108] Han J, Richardella A, Siddiqui S A, Finley J, Samarth N and Liu L 2017 Room-temperature spin–orbit torque switching induced by a topological insulator *Phys. Rev. Lett.* **119** 077702

[109] Liu L, Pai C-F, Li Y, Tseng H W, Ralph D C and Buhrman R A 2012 Spin-torque switching with the giant spin hall effect of tantalum *Science* **336** 555–8

[110] Liu L, Moriyama T, Ralph D C and Buhrman R A 2011 Spin-torque ferromagnetic resonance induced by the spin hall effect *Phys. Rev. Lett.* **106** 036601

[111] Pai C-F, Liu L, Li Y, Tseng H W, Ralph D C and Buhrman R A 2012 Spin transfer torque devices utilizing the giant spin Hall effect of tungsten *Appl. Phys. Lett.* **101** 122404

[112] Zhang H *et al* 2023 Fermi-level-dependent charge-to-spin conversion of the two-dimensional electron gas at the γ-Al$_2$O$_3$/KTaO$_3$ interface *Phys. Rev. Appl.* **19** 034045

[113] Miron I M, Garello K, Gaudin G, Zermatten P-J, Costache M V, Auffret S, Bandiera S, Rodmacq B, Schuhl A and Gambardella P 2011 Perpendicular switching of a single ferromagnetic layer induced by in-plane current injection *Nature* **476** 189–93

[114] Garello K, Miron I M, Avci C O, Freimuth F, Mokrousov Y, Blügel S, Auffret S, Boulle O, Gaudin G and Gambardella P 2013 Symmetry and magnitude of spin–orbit torques in ferromagnetic heterostructures *Nat. Nanotechnol.* **8** 587–93

[115] Hayashi M, Kim J, Yamanouchi M and Ohno H 2014 Quantitative characterization of the spin–orbit torque using harmonic Hall voltage measurements *Phys. Rev.* B **89** 144425

[116] Prenat G, Jabeur K, Di Pendina G, Boulle O and Gaudin G 2015 Beyond STT-MRAM, spin–orbit Torque RAM SOT-MRAM for high speed and high reliability applications *Spintronics-based Comput.* 145–57

[117] Narayanapillai K, Gopinadhan K, Qiu X, Annadi A, Ariando, Venkatesan T and Yang H 2014 Current-driven spin–orbit field in LaAlO$_3$/SrTiO$_3$ heterostructures *Appl. Phys. Lett.* **105** 162405

[118] Vaz D C, Trier F, Dyrdał A, Johansson A, Garcia K, Barthélémy A, Mertig I, Barnaś J, Fert A and Bibes M 2020 Determining the Rashba parameter from the bilinear magnetoresistance response in a two-dimensional electron gas *Phys. Rev. Mater.* **4** 071001

[119] Choe D *et al* 2019 Gate-tunable giant nonreciprocal charge transport in noncentrosymmetric oxide interfaces *Nat. Commun.* **10** 4510

[120] Zhang J *et al* 2021 Anisotropic bilinear magnetoresistance in (110) SrTiO$_3$-based two-dimensional electron gas *Phys. Rev.* B **104** 045114

[121] Jin M-J *et al* 2017 Nonlocal spin diffusion driven by giant spin hall effect at oxide heterointerfaces *Nano Lett.* **17** 36–43

[122] Sinova J, Culcer D, Niu Q, Sinitsyn N A, Jungwirth T and MacDonald A H 2004 Universal intrinsic spin hall effect *Phys. Rev. Lett.* **92** 126603

[123] Trier F *et al* 2020 Electric-field control of spin current generation and detection in ferromagnet-free SrTiO$_3$-based nanodevices *Nano Lett.* **20** 395–401

[124] Hwang H Y, Iwasa Y, Kawasaki M, Keimer B, Nagaosa N and Tokura Y 2012 Emergent phenomena at oxide interfaces *Nat. Mater.* **11** 103–13

[125] Manipatruni S, Nikonov D E, Lin C-C, Gosavi T A, Liu H, Prasad B, Huang Y-L, Bonturim E, Ramesh R and Young I A 2019 Scalable energy-efficient magnetoelectric spin–orbit logic *Nature* **565** 35–42